eNeuro

Research Article: New Research | Cognition and Behavior

Sex-specific role for dopamine receptor D2 in dorsal raphe serotonergic neuron modulation of defensive acoustic startle and dominance behavior

https://doi.org/10.1523/ENEURO.0202-20.2020

Cite as: eNeuro 2020; 10.1523/ENEURO.0202-20.2020

Received: 19 May 2020
Revised: 19 October 2020
Accepted: 9 November 2020

1. Manuscript Title (50 word maximum)
Sex-specific role for dopamine receptor D2 in dorsal raphe serotonergic neuron modulation of defensive acoustic startle and dominance behavior

2. Abbreviated title (50 character maximum)
DRD2 in serotonergic neuron modulation of behavior

3. List all Author Names and Affiliations in order as they would appear in the published article
Krissy A. Lyon[1], Benjamin D. Rood[1], Lorna Wu[2], Rebecca A. Senft[1], Lisa V. Goodrich[2], and Susan M. Dymecki[1]
[1]Department of Genetics, Harvard Medical School, Boston, Massachusetts 02115, and
[2]Department of Neurobiology, Harvard Medical School, Boston, Massachusetts 02115

4. Author contributions:
KAL and SMD designed research; KAL, BDR, and LW Performed Research; KAL, BDR, RAS, and SMD analyzed data, LVG, RAS contributed analytic tools; KAL and SMD wrote paper

5. Correspondence should be addressed to (include email address)
Susan M. Dymecki, Department of Genetics, Harvard Medical School, 77 Avenue Louis Pasteur, New Research Building, Boston, MA 02115. dymecki@genetics.med.harvard.edu

6. Number of figures: 10
7. Number of tables : 2
8. Number of multimedia: None
9. Number of words for Abstract: 249
10. Number of words for Significance statement: 118
11. Number of words for introduction: 697
12. Number of words for discussion: 1678

13. Acknowledgements: This work was supported by the National Institutes of Health (National Institute on Drug Abuse Grant R01 DA034022 to S.M.D; Blueprint Award NS108515 to K.A.L) and G.V.R. Khodadad Fund for studies of EPS to S.M.D. K.A.L. was a Howard Hughes Medical Institute Gilliam Fellow. Most behavioral work was carried out in the NeuroBehavior Laboratory Core at Harvard Medical School, we appreciate the support of Director Dr. Barbara Caldarone. We thank all S.M.D. laboratory members, including G. Maddaloni, B. Okaty, R. Dosumu-Johnson, Lehigh, K. and T. Asher, for discussions. O. Alekseyenko for discussion and behavioral assay support. K. Blandino, B. Menjivar and J. Mai for technical support. B. Shrestha for auditory brainstem response assistance. The Microscopy Resources on the North Quad (MicRoN) core at Harvard Medical School for microscopy support. Graphical abstract and tube test diagram created with BioRender.com.

B. Rood's present address: Department of Cell Biology & Neuroscience, Rowan University, Stratford, NJ

14. **Conflict of interest**: Authors declare no competing financial interests.

15. Funding sources: National Institutes of Health: National Institute on Drug Abuse Grant R01 DA034022; Blueprint Award NS108515; National Institute on Deafness and Other Communication R01 DC015974; G.V.R. Khodadad Fund for studies of EPS.

Abstract: Brain networks underlying states of social and sensory alertness are normally adaptive, influenced by serotonin and dopamine, and abnormal in neuropsychiatric disorders, often with sex-specific manifestations. Underlying circuits, cells, and molecules are just beginning to be delineated. Implicated is a subtype of serotonergic neuron denoted *Drd2-Pet1* –distinguished by expression of the type-2 dopamine receptor (*Drd2*) gene, inhibited cell-autonomously by DRD2 agonism in slice, and, when constitutively silenced in male mice, affects levels of defensive and exploratory behaviors (Niederkofler et al., 2016). Unknown has been whether DRD2 signaling in these *Pet1* neurons contributes to their capacity for shaping defensive behaviors. To address this, we generated mice in which *Drd2* gene sequences were deleted selectively in *Pet1* neurons. We found that $Drd2^{Pet1\text{-}CKO}$ males, but not females, demonstrated increased winning against sex-matched controls in a social dominance assay. $Drd2^{Pet1\text{-}CKO}$ females, but not males, exhibited blunting of the acoustic startle response – a protective, defensive reflex. Indistinguishable from controls were auditory brainstem responses, locomotion, cognition, and anxiety- and depression-like behaviors. Analyzing wild-type *Drd2-Pet1* neurons, we found sex-specific differences in the proportional distribution of axonal collaterals, in action potential duration, and in transcript levels of *Gad2,* important for GABA synthesis. $Drd2^{Pet1\text{-}CKO}$ cells displayed sex-specific differences in the percentage of cells harboring *Gad2* transcripts. Our results suggest that DRD2 function in *Drd2-Pet1* neurons is required for normal defensive/protective behaviors in a sex-specific manner, which may be influenced by the identified sex-specific molecular and cellular features. Related behaviors in humans too show sex differences, suggesting translational relevance.

Significance statement

A subtype of dorsal raphe serotonergic neuron, denoted *Drd2-Pet1*, is poised for regulation by dopamine via type-2 dopamine receptor (DRD2) expression. Functional removal of DRD2 in these cells through a conditional knockout (CKO) mouse strategy resulted in sex-specific behavioral abnormalities: $Drd2^{Pet1\text{-}CKO}$ females exhibited reduced acoustic startle while males showed increased social dominance. *Drd2-Pet1* neurons were similar in number and distribution in males versus females but exhibited sex-specific differences in neurotransmission-related mRNAs, action potential duration, and relative distribution of collaterals. Abnormalities in sensory processing and social behaviors akin to those reported here manifest in autism, schizophrenia, and post-traumatic stress disorder, in sex-specific ways. Our findings, thus, may point to novel circuits and modulatory pathways relevant to human neuropsychiatric conditions.

Introduction

The serotonergic and dopaminergic neurotransmitter systems are known for their influence on and maladaptation in neuropsychiatric disorders, including post-traumatic stress disorder, autism spectrum disorder, and schizophrenia. Clinical and animal studies implicate serotonin (5-hydroxytryptamine, 5-HT) and dopamine (DA) in modulation of endophenotypes common to neuropsychiatric disorders, such as altered social interaction and sensory processing (Geyer and Braff, 1987; Meincke et al., 2004; Takahashi and Kamio, 2018). Transcriptome data coupled with structure-function maps in mice show that the serotonergic and dopaminergic neuronal systems are themselves heterogeneous, comprised of functionally specialized neuronal subtypes, manifesting distinct mRNA profiles, efferent projections, electrophysiological properties, and

functions (Jensen et al., 2008; Kim et al., 2009; Crawford et al., 2013; Lammel et al., 2014; Spaethling et al., 2014; Okaty et al., 2015; Deneris and Gaspar, 2018; Poulin et al., 2018; Huang et al., 2019; Ren et al., 2019; Poulin et al., 2020). An important subtype of serotonergic neuron as relates to social and defensive behaviors is denoted *Drd2-Pet1* (Niederkofler et al., 2016), identified by expression of the type-2 dopamine receptor (*Drd2*) gene and the serotonergic transcription factor gene *Pet1 (*aka *Fev)*. DRD2 agonism in slice preparation drove outward (inhibitory) currents cell-autonomously in *Drd2-Pet1* neurons, suppressing their excitability; and when these cells were constitutively silenced in male mice –i.e. exocytic neurotransmitter release was cell autonomously blocked – defensive, aggressive, and exploratory behaviors increased (Niederkofler et al., 2016). Here we query whether *Drd2* expression in *Drd2-Pet1* cells contributes to the modulation of defensive, exploratory behaviors.

While *Drd2* is expressed in many cell types throughout the midbrain and basal forebrain, expression in serotonergic neurons is restricted to a small subset of cells resident in the dorsal raphe (DR) nucleus. In these serotonergic neurons, *Drd2* expression initiates around adolescence and continues through adulthood, at which point, *Drd2* transcripts are the major DA receptor mRNA detected (Niederkofler et al., 2016). Thus *Drd2-Pet1* neurons come under DRD2 and presumably DA regulation during the developmental transition to sexual maturity. *Drd2-Pet1* neurons project to brain regions involved in sensory processing, defensive, and mating behaviors including auditory brainstem regions and the sexually dimorphic medial preoptic area (Niederkofler et al., 2016).These findings led us to hypothesize that DRD2 signaling in

120 *Drd2-Pet1* neurons contributes to social and sensory alertness and defensive behavior
121 in a sex-specific manner.

122 Indeed, serotonergic and dopaminergic perturbations affect social and defensive
123 behaviors differently in male versus female rodents. Decreases in serotonergic tone
124 associate with increased levels of aggression in males (Brown et al., 1982; Hendricks et
125 al., 2003; Yu et al., 2014; Niederkofler et al., 2016). By contrast, lesions of the
126 serotonergic DR in female rats decreased maternal aggression (Holschbach et al.,
127 2018), while DR serotonergic neuron activity in female, but not male, hamsters
128 associates with social dominance (Terranova et al., 2016). The acoustic startle reflex
129 (ASR) – an evolutionarily-conserved, defensive reflex to loud, potentially threatening
130 stimuli (Davis et al., 1982) – also shows sex-specific differences within the context of
131 altered 5-HT levels. Reduction in 5-HT levels enhanced ASR in female but not male rats
132 (Pettersson et al., 2016). With respect to DA, deletion of the DA re-uptake transporter
133 gene (*Dat*) altered ASR only in male mice (Ralph et al., 2001). Genetic removal of the
134 soluble form of catechol-O-methyltransferase (COMT), important for degradation of DA,
135 enhanced the ASR and dominance behaviors in both sexes, but ASR especially in
136 males (Tammimaki et al., 2010). Thus, serotonergic and dopaminergic neuronal
137 systems influence social behaviors and sensory processing in sex-specific ways.

138 Here we queried whether *Drd2* conditional deletion in serotonergic neurons
139 would alter aggression and social dominance behavior in males. Further, we sought to
140 examine the role of *Drd2* expression in serotonergic neurons in females with the
141 hypothesis that other sensory or defensive behaviors would be affected, given typical
142 lack of aggression in female mice (Lonstein and Gammie, 2002). We undertook a

phenotypic analysis of mice in which we engineered *Drd2* gene deletion selectively in *ePet1-cre*-expressing serotonergic neurons (*Drd2*$^{Pet1\text{-CKO}}$ mice). Here, we report that *Drd2*$^{Pet1\text{-CKO}}$ males exhibited increased social dominance whereas females displayed a robust decrease in ASR. We also investigated sex differences in *Drd2-Pet1* neurons at the molecular, cellular, and circuit levels, identifying differences in candidate mRNA levels, electrophysiological properties, and relative distribution densities of axonal collaterals.

Materials and Methods

Ethical approval

All experimental protocols were approved by Harvard University Institutional Animal Care and Use Committees (IACUC) and were in accordance with the animal care guidelines of the National Institutes of Health.

Experimental animals

Mice were housed in a temperature-controlled environment on a 12:12 hour light-dark cycle with *ad libitum* access to standard mouse chow and water. All experimental animals were virgins. For conditional knockout of *Drd2,* double transgenic mice of the genotype *ePet-Cre;Drd2*$^{loxP/loxP}$ (referred to as *Drd2*$^{Pet1\text{-CKO}}$) were generated by crossing BAC transgenic *ePet-Cre* (Scott et al., 2005) (Jax #012712) males to homozygous *Drd2*$^{loxP/loxP}$ (Bello et al., 2011) (Jax #020631) females. From these crosses, *ePet-Cre;Drd2*$^{loxP/wildtype}$ males were then bred to homozygous *Drd2*$^{loxP/loxP}$ females for *ePet-Cre;Drd2*$^{loxP/loxP}$ male and female offspring used for experiments. Experimental controls were littermates with the *Drd2*$^{loxP/loxP}$ genotype thus negative for Cre but of comparable genetic background (C57BL/6J, Jax #000664). For *Drd2-Pet1* neuron cell counts, triple

transgenic *Drd2-Cre;Pet1-Flpe;RC-FrePe* (Gong et al., 2007; Jensen et al., 2008; Brust et al., 2014) (*RC-FrePe* Jax #029486) were generated by crossing *Drd2-Cre* females to *Pet1-Flpe;RC-FrePe* double transgenic males. Likewise for axonal projection mapping, *Drd2-Cre; Pet1-Flpe; RC-FPSit* (*RC-FPSit* Jax #030206) triple transgenic mice were generated by crossing *Drd2:Cre* females to *Pet1-Flpe;RC-FPSit* double transgenic males. For both *RC-FrePe* and *RC-FPSit* crosses, all animals of each sex were from separate litters, though males and females from the same litter were used when possible. Genotypes were determined as previously described (Brust et al., 2014). Number of animals used for each assay is listed under the description for each assay.

Immunohistochemistry

Mice were briefly anesthetized with isoflurane and immediately perfused intracardially with phosphate buffered saline (PBS) followed by 4% paraformaldehyde (PFA) in PBS. Brains were extracted, post-fixed in 4% PFA overnight at 4˚C, cryoprotected in 30% sucrose/PBS for 48 hours, and embedded in OCT compound (Tissue-Tek). Coronal sections were cryosectioned as 30 µm free-floating sections then rinsed three times with PBS for 10 minutes, blocked in 5% normal donkey serum (NDS, Jackson ImmunoResearch) and permeabilized with 0.1% Triton X-100 in PBS for 1 hour at room temperature. Sections were incubated for 24-48 hours in primary antibodies in the same blocking buffer at 4˚C. Primary antibodies used were goat polyclonal anti-5-HT (1:1000, Cat #ab66047; Abcam), chicken polyclonal anti-GFP (1:2000, RRID: AB_2307313, AVES), rabbit polyclonal anti-DsRed (1:1000; Cat #632496; Clontech) and rabbit anti-GABA (1:500, Cat# A2052, Sigma). Following primary antibody incubation, sections were rinsed three times with PBS for 10 minutes and incubated in secondary antibody

(Alexa Fluor 488 Donkey anti-Chicken IgY, 703-545-155, Jackson ImmunoResearch; Alexa Fluor 546 Donkey anti-Rabbit IgG, A10040, Invitrogen; Alexa Fluor 647 Donkey anti-Goat IgG, A-21447, Invitrogen) for 1 hour at room temperature, rinsed three times with PBS for 10 minutes, then mounted using ProLong Gold Antifade Mountant (P36930, LifeTechnologies). For *Drd2-Pet1* neuron cell counts, GFP+ cells were counted in every 6th section. The resulting number was multiplied by 6 to obtain the number of *Drd2-Pet1* cells per animal.

Dual immunohistochemistry and fluorescent *in situ* hybridization

For dual *in situ* hybridization with immunostaining for GFP+ *Drd2-Pet1* neuron cell bodies, PFA-perfused brain tissue from adult *Drd2-Cre;Pet1-Flpe;RC-FrePe* mice was collected as described above but cryosectioned at 20 µm onto slides (Superfrost Plus, Ca no. 48311-703, VWR), slides were warmed on a slide warmer set to 45˚C for 30 minutes, and processed with RNAscope Multiplex Fluorescent Assay Kit (Advanced Cell Diagnostics) following manufacturer's protocol with the exception that at the end of the protocol, tissue was stained for anti-GFP, as described above, similar to (Shrestha et al., 2018). The following probes were used for the dual protocol: *Dmd* (Cat. # 561551-C3), *Drd2-E2* (Cat. # 486571-C2 or -C3), *Gad2* (Cat. # 439371-C2), and *Serpini1* (Cat. # 501441). Cell nuclei were visualized with DAPI (4',6-diamidino-2-phenylindole).

Fluorescent *in situ* hybridization

For fluorescent *in situ* hybridization validation of *Drd2* conditional knockout and *Gad2* expression analysis, adult *Drd2*$^{Pet1\text{-}CKO}$ or control brain tissue was fresh frozen in OCT (TissueTek) and cryosectioned at 16 µm onto slides (Superfrost Plus, Ca no. 48311-703, VWR) and then processed with RNAscope Multiplex Fluorescent Assay Kit

(Advanced Cell Diagonstics) following manufacturer's protocol for fresh frozen tissue. The following probes were used: *Drd2-E2* (Cat. # 486571-C2), *Drd2*-O4 (Exon7/8) (Cat #534241), *Fev (Pet1)* (Cat. # 413241-C3), *Gad2* (Cat. #439371-C2), *Tph2* (Cat # 318691), and *cre* (Cat. # 312281). Cell nuclei were visualized with DAPI (4',6-diamidino-2-phenylindole).

Image collection

All images were acquired on a Nikon Ti inverted spinning disk confocal microscope with 488, 561, 647 nm laser lines and Andor Zyla 4.2 Plus sCMOS monochrome camera. Images were acquired with Nikon Elements Acquisition software AR 5.02. For RNA quantification and *Drd2*$^{Pet1\text{-}CKO}$ validation experiments, four images were taken of brain slices containing the DR: the first directly ventral to the aqueduct then one field of view below and to the left and right to capture each lateral wing.

Fluorescent *in situ* hybridization (FISH) quantification

Quantification was conducted blind to sex and genotype. For *Drd2*$^{Pet1\text{-}CKO}$ validation, all *Pet1*+ (serotonergic) neurons within each image were identified, then the viewer outlined the DAPI stained nuclei of each *Pet1*+ neuron and scored the presence of *Drd2* puncta as 'positive' (having puncta) or 'negative' (no puncta).The total number of *Drd2*+ *Pet1*+ neurons was then divided by the total number of *Pet1*+ neurons to yield the '% *Drd2*+*Pet1*+ neurons'.

For quantification of *Dmd, Drd2, Gad2,* and *Serpini* manual counting of each mRNA punctum per cell was conducted by a trained viewer. All cells counted fit the criteria of GFP+ with a DAPI+ nucleus. The viewer outlined the GFP+ cell body in Fiji (http:fiji.sc/Fiji) (Schindelin et al., 2012) while only viewing that channel and then

counted the number of distinct RNA puncta within that cell outline. Brain sections sampled were from 5 males and 5 female animals.

For quantification of *Drd2*-Exon7/8 and *Gad2* puncta in *Drd2*$^{Pet1\text{-}CKO}$ tissue, DR sections corresponded to interaural -0.80 mm to 1.04 mm and Bregma -4.60 to – 4.84 based on DAPI staining and anatomical landmarks (Franklin and Paxinos, 2008), where *Drd2-Pet1* neurons are most enriched. A series of custom Fiji scripts and a CellProfiler (McQuin et al., 2018) pipeline were used to process and analyze confocal images of RNAscope FISH signal in a semi-automatic manner. Analysis was performed in 2D on maximum intensity projections of 6 µm thick z-stacks. First, a (Step 1) preprocessing Fiji script separated channels and preprocessed them for (Step 2) CellProfiler to use as input to segment nuclei. The DAPI-stained channel was preprocessed by a gaussian blur with a diameter of 18 before segmenting with the IdentifyPrimaryObjects module with a diameter range 30-100 pixels using a minimum cross entropy global thresholding strategy. Objects outside of the diameter range or those on the edges were excluded. A threshold smoothing scale of 1.3488 was used and the image was automatically declumped based on intensity values. Finally, holes were filled in the resulting label map image, which was exported for use in FIJI (Step 3). In FIJI, the user manually excluded misidentified objects or added additional nuclei that were missed by the automatic detection pipeline. A highly similar script was recently published (Okaty et al., 2020), though this current script performs additional difference of gaussian (Marr and Hildreth, 1980) based filtering for each FISH channel. For each FISH probe, after background subtraction with a rolling ball radius of 50 pixels, the image was duplicated and a gaussian blur was performed at two different sigma levels, one which obscured small

background pixels but preserved mRNA puncta, and a more extreme blur that only retained larger diffuse background puncta. The difference of these two images was then calculated and puncta localized using the Find Maxima function. To find appropriate settings for each FISH channel, we compared the performance of several sets of parameters to automatically detect puncta vs. a hand count of puncta. We were able to achieve excellent concordance between the hand count and automatic puncta detection. Table 1 summarizes our settings and performance in a linear regression against the hand count for each FISH probe (statistics calculated in GraphPad Prism v8.4.3 and Microsoft Excel v2002).

Behavioral assays

All assays, except the resident intruder assay, were conducted in an initial cohort of 15 control (8 males, 7 females) and 11 *Drd2*$^{Pet1\text{-}CKO}$ (6 males, 5 females) mice. All behavioral assays were conducted at P90 or later. The run order for the initial cohort was open field, elevated plus maze, tail suspension test, forced swim test, social interaction, acoustic startle response, paired pulse inhibition of acoustic startle, water T-maze, contextual fear conditioning, tube test of social dominance and rotarod. An additional cohort of 16 controls (7 males, 9 females) *Drd2*$^{Pet1\text{-}CKO}$ (6 males, 10 females) was run for acoustic startle response. Resident intruder assay of aggression was conducted in three separate cohorts of mice totaling 24 control and 26 *Drd2*$^{Pet1\text{-}CKO}$ males. The tube test of social dominance was run in the initial cohort and in the second (8 control and *Drd2*$^{Pet1\text{-}CKO}$ males) and third (11 control and *Drd2*$^{Pet1\text{-}CKO}$ males) aggression cohorts for a total of 24 control and *Drd2*$^{Pet1\text{-}CKO}$ males and a separate cohort of 16 control and 18 *Drd2*$^{Pet1\text{-}CKO}$ females. The rotarod assay was also repeated

281 in a separate cohort of males (7 controls, 6 *Drd2*$^{Pet1\text{-}CKO}$). Experiments were conducted
282 between ZT6-10, with interspersion of control and experimental animals, and assays
283 were run and analyzed by a trained experimenter blinded to genotype. The open field
284 test, elevated plus maze, tail suspension test, forced swim test, social interaction, paired
285 pulse inhibition of acoustic startle, water T-maze, and contextual fear conditioning were
286 performed as previously described (Niederkofler et al., 2016). All other behavioral
287 assays are described in detail below.
288 Rotarod: The rotarod apparatus (Stoelting; Ugo Basile Apparatus) contains a rotating
289 rod set to an accelerating speed. Mice are placed onto the rod and rotation of the rod
290 begins. When a mouse loses its balance and falls, the apparatus automatically stops
291 and measures the latency and rotating speed at which the mouse fell. Training
292 consisted of exposing the mice to the apparatus for 5 minutes at a constant speed of 4
293 rpm. Mice that fall during the training session are placed back on the apparatus until the
294 training session time has elapsed. An hour following the training session, mice are
295 placed back on the rod for a 2-minute session in which speed increases steadily over 2
296 minutes from 5-40 rpm. If a mouse does not fall during the 2 minutes, the trial ends at 2
297 minutes. Each animal was tested over 3 days and the latency to fall was averaged for
298 each mouse. This assay was conducted in 21 control mice (14 males, 7 females) and
299 18 *Drd2*$^{Pet1\text{-}CKO}$ (13 males, 5 females).
300 Acoustic Startle Response: Mice were placed in a perforated holder (acrylic cylinder
301 with 3.2 cm internal diameter) that allowed movement to be monitored. Animal holders
302 were placed on top of a transducer platform, measuring the active response to both
303 weak and startle stimuli, adjacent to a speaker, within an individual acoustic chamber

(Med Associates, see schematic diagram in Fig. 3B). Each session consisted of a five-minute acclimation period followed by 10 blocks of 11 trials each with white noise acoustic stimuli (20-120 dB). Each startle stimulus (20-120 dB, in 10 dB increments) was played once per block, in a quasi-random order with a variable inter-trial interval of 10-20 seconds (average of 15 seconds). The duration of the stimulus was 40 ms. Responses were recorded for 150 ms from startle onset and are sampled every ms. Mice were placed back into the home cage immediately after testing. Males and female were run on different days. This assay was conducted in 30 control mice (14 males, 16 females) and 28 *Drd2*$^{Pet1\text{-}CKO}$ (13 males, 15 females), as two separate cohorts per sex.

Tube Test of Social Dominance: Two age-matched (~P90), weight-matched mice of the same sex are introduced into opposite ends of a clear PVC tube (30.5 cm in length with an internal diameter of 2.5 cm) allowing them to interact in the middle but not pass each other within the tube. The subordinate mouse will back out allowing the dominant mouse to pass through (Lindzey et al., 1961). For each pair, five consecutive trials were run with a maximum time of 2 minutes per trial. Trials ended when one mouse backed out of the tube such that all four limbs are outside of the tube which was then recorded as a 'backout' for that mouse. Matches lasting more than two minutes were excluded from analysis and scored as a draw. Side of introduction to the tube were alternated between trials and the tube was cleaned with ethanol between each trial. Opponents were from different litters and had never been housed together. This assay was conducted in 24 *Drd2*$^{Pet1\text{-}CKO}$ males versus 24 control males and 23 *Drd2*$^{Pet1\text{-}CKO}$ females versus 23 control females, conducted across 3 cohorts of animals.

Resident Intruder Assay: *Drd2*$^{Pet1\text{-}CKO}$ or control mice were group-housed with male siblings until adulthood (P90) when they were single-housed for one night in the test cage to establish territorial residency. On day 1, a 5-week old Swiss Webster (Charles River) male, the "intruder", was introduced to the cage divided with a clear perforated divider for five minutes. After five minutes, the perforated divider was removed, and the mice could interact for 5 minutes, in which the encounter was video recorded. Number of attack bites were counted by a trained, blinded viewer. The intruder mouse was introduced for 3 days to obtain an average number of attack bites per day. The intruder mouse had a lower body weight than the resident male. This assay was conducted only in males, as female laboratory-reared mice do not display territorial aggression (Palanza, 2001; Lonstein and Gammie, 2002) This assay was conducted in 26 *Drd2*$^{Pet1\text{-}CKO}$ and 24 controls.

Auditory Brainstem Response (ABR): ABRs were recorded in a separate cohort of adult mice (males: 10 control and 7 *Drd2*$^{Pet1\text{-}CKO}$; females: 8 control and 7 *Drd2*$^{Pet1\text{-}CKO}$) aged P71-102 to correspond to the age of animals in other assays. ABRs were conducted similar to (Maison et al., 2013). Mice were anesthetized by intraperitoneal injection of ketamine (100 mg/kg) and xylazine (7.5 mg/kg) and placed in a soundproof chamber on a heating pad. Acoustic stimuli were delivered using EPL Cochlear Function Test Suite (CFTS) software and analyzed using ABR peak analysis software (1.1.1.9, Massachusetts Eye and Ear (MEE)). All ABR thresholds, amplitudes, and latencies were read by an investigator blind to mouse genotype.

Electrophysiology

Slice preparation and whole cell patch clamp recordings were conducted as previously

described (Rood et al., 2014; Niederkofler et al., 2016). Briefly, to assess membrane and action potential characteristics a protocol of repeated sweeps of 500 ms current injections stepping in 20 pA steps from -80 pA to 180 pA was administered to cells in current clamp. Data were analyzed using Clampfit (Molecular Devices, San Jose, CA). Some cells included in cell property analyses were also used to generate data on the function of DRD2 receptors in the DR (Niederkofler et al., 2016). However, the intrinsic cell properties data we present in this article have not been previously published and include cells not part of the Niederkofler et al. (2016) dataset.

Projection mapping

Brain tissue from 6 females and 5 males from different litters, but with a female and male from the same litter where possible, were collected at P90 and processed as previously described (Niederkofler et al., 2016). Target region identification was based on anatomical landmarks identified by DAPI staining, anti-choline acetyltransferase (Goat polyclonal anti-ChAT,1:500, AB144P; EMD234 Millipore) staining, and/or anti-tyrosine hydroxylase (rabbit anti-TH, 1:1000, AB152, Millipore) staining. Staining and imaging protocols were identical amongst the eleven samples analyzed.

Quantification of target innervation

Target innervation was quantified in a similar manner to (Niederkofler et al., 2016). Briefly, image stacks were acquired bilaterally per brain region analyzed for each animal using a Nikon Ti inverted spinning disk microscope with a Plan Fluor 40x/1.3 Oil DIC H/N2 objective, 488, 561, and 647 nm laser lines, and Andor Zyla 4.2 Plus sCMOS monochrome camera. Images were acquired with Nikon Elements Acquisition software AR 5.02. Image stacks (.nd2 files) were imported to Fiji for analysis of axon projection

area. Each stack contained 21 optical slices of 0.3 µm. Innervation density was quantified by a Fiji macro, such that all images, were treated identically, including background subtraction, thresholding and particle counting as described in (Niederkofler et al., 2016). We then divided the total area occupied by the projection signal by the total area of the 21 optical slices to obtain the percent area occupied by projection signal. This was then averaged within images of the same brain region across male or female samples. Brain regions analyzed were either those previously described to be innervated by *Drd2-Pet1* neurons in males only (Niederkofler et al., 2016) or those involved in auditory processing and ASR.

Statistical analyses

Data are presented as mean ± standard error of the mean (SEM). Statistical analyses were conducted in GraphPad Prism Version 8.1. Statistical significance was determined by unpaired T-test between control versus $Drd2^{Pet1\text{-}CKO}$ groups or male versus female groups except where noted: Open field, forced swim test, acoustic startle response, and auditory brainstem response statistical significance was determined using two-way ANOVA. For the resident intruder assay, the tube test of social dominance, and rotarod, statistical significance was determined using the non-parametric Mann-Whitney U test. A result was considered significant if the p value was <0.05. Detailed statistical results are reported in Table 2.

Results

Visualization of *Drd2-Pet1* serotonergic neurons and the loss of *Drd2* gene expression in $Drd2^{Pet1\text{-}CKO}$ mice

As our first step, we confirmed the anatomical distribution of *Drd2-Pet1* neurons in the mouse brainstem, observing cell soma distributed across the rostral and lateral regions of the dorsal raphe (DR) nucleus (Fig. 1A) as previously reported (Niederkofler et al., 2016). *Drd2-Pet1* cells were marked by GFP expression in triple transgenic *Drd2-cre* (Gong et al., 2007), *Pet1-Flpe* (Jensen et al., 2008), *RC-FrePe* (Brust et al., 2014) mice in which cells positive for both Cre and Flpe activity – here those cells having expressed *Drd2* and *Pet1* – have recombined the *RC-FrePe* intersectional reporter allowing GFP expression; Flpe recombination alone configured *RC-FrePe* to drive mCherry expression, thus marking the remaining *Pet1*+ (*Drd2*-negative) serotonergic neurons (Fig. 1A-B). As expected (Niederkofler et al., 2016), GFP+ *Drd2-Pet1* neurons showed detectable 5-HT by immunostaining and *Drd2* mRNA by fluorescent *in situ* hybridization (Fig. 1C).

To query the behavioral requirement for *Drd2* gene expression in *Drd2-Pet1* neurons, we deployed the e*Pet-cre* driver (Scott et al., 2005) to delete floxed *Drd2* gene sequences (Bello et al., 2011), creating a functional null *Drd2* allele selectively in *Pet1* neurons (Fig. 1D), and then subjected these $Drd2^{Pet1\text{-}CKO}$ mice to behavioral phenotyping. Cre-negative, $Drd2^{flox/flox}$ littermates served as controls. To confirm loss of *Drd2* gene expression in *Pet1* neurons, we analyzed $Drd2^{Pet1\text{-}CKO}$ and control $Drd2^{flox/flox}$ brain tissue sections by mRNA *in situ* hybridization using a probe designed to detect exon 2-containing *Drd2* mRNA, as exon 2 was the floxed gene portion to be excised by Cre recombination; concomitant identification of serotonergic neurons was by detection of *Pet1* transcripts (Fig. 1F-G). Robust loss of *Drd2* expression was observed in serotonergic neurons in both male and female mice (Fig. 1E, 15.23% ± 2.41 of *Pet1*+

417 neurons in the DR express *Drd2* transcripts in controls (n=6), consistent with prior
418 findings, compared to 3.87% ± 0.73 in *Drd2*$^{Pet1\text{-CKO}}$s (n=6), p=0.0011, unpaired T-test).
419 The few residual *Pet1*+ cells harboring *Drd2* transcripts likely reflects a limitation in cell
420 capture by the *ePet-cre* driver. Reliable immunodetection to confirm the expected
421 parallel loss of DRD2 protein in PET1 cells remains unavailable.

422 **Behavioral assessments in *Drd2*$^{Pet1\text{-}CKO}$ mice and the detection of sex-specific**
423 **sensory, defensive, and social behaviors**

424 Having validated effective loss of *Drd2* expression specific to *Pet1* neurons in
425 *Drd2*$^{Pet1\text{-CKO}}$ mice, next we screened these mice for behavioral alterations in comparison
426 to sibling control *Drd2*$^{flox/flox}$ (Cre-negative) mice. Locomotor behaviors were explored
427 first because they are known to be influenced by serotonergic and dopaminergic
428 manipulations (Baik et al., 1995; Gainetdinov et al., 1999; Holmes et al., 2003; Seo et
429 al., 2019), and because motor alterations can affect performance in and interpretation of
430 subsequent behavioral assays. Notably, we found no differences between *Drd2*$^{Pet1\text{-CKO}}$
431 versus control mice (males or females) in the locomotor behaviors reflected in the open
432 field and rotarod tests, such as distance traversed (Fig. 2A) and location within the field
433 (Fig. 2B), vertical rearing, length of time on the rotating rod (Fig. 2C), which reflects
434 balance, coordination, physical conditioning, and motor-planning. Next, we explored
435 measures of depression- and anxiety-like behaviors, as they are altered in various 5-
436 HT- or DA-pathway mouse models and pharmacological manipulation of these
437 neurotransmitter systems show positive clinical effect. (Lucki, 1998; Hendricks et al.,
438 2003; Holmes et al., 2003; Grace, 2016). We observed no differences in performance in
439 the elevated plus maze (Fig. 2D), tail suspension test (Fig. 2E), or forced swim test (Fig.

2F) in *Drd2*$^{Pet1\text{-}CKO}$ males and females compared to littermate controls. Additionally, contextual fear conditioning (Fig. 2G) and water T-maze acquisition and reversal (Fig. 2H) were not affected, suggesting no impairment of memory and learning in *Drd2*$^{Pet1\text{-}CKO}$ mice.

Because the serotonergic and dopaminergic systems are implicated in modulating the ASR (Davis and Aghajanian, 1976; Davis et al., 1980; Meloni and Davis, 1999; Meloni and Davis, 2000b; Meloni and Davis, 2000a), we explored that next. The ASR is an evolutionarily conserved reflex involving rapid contraction of facial and skeletal muscles into a protective posture in response to a loud, threatening stimulus. We hypothesized that *Drd2-Pet1* neurons modulate this response, given their dense projections to auditory brain regions (Niederkofler et al., 2016) and the observation that following acoustic startle, the activity of certain serotonergic neurons increases in the lateral-wings of the DR (Spannuth et al., 2011) – a location in which we find *Drd2-Pet1* neurons. We measured startle responses to weak and startling stimuli ranging from 20 to 120 decibel (dB) presented in a randomized order (Fig. 3A-B). Female *Drd2*$^{Pet1\text{-}CKO}$ mice showed a significant decrease in ASR magnitude in response to startle stimuli (Fig. 3F, n=15 *Drd2*$^{Pet1\text{-}CKO}$, n=16 control littermates, p=0.0011, Two-way ANOVA). By contrast, the male *Drd2*$^{Pet1\text{-}CKO}$ cohort was indistinguishable from their male littermate controls (Fig. 3C, n=13 *Drd2*$^{Pet1\text{-}CKO}$, n=14 control littermates, p=0.7745, Two-way ANOVA). To prevent habituation to the startle stimuli, the different stimulus intensities were presented in a quasi-random order with varied inter-trial intervals (see methods), and indeed, startle responses in late as compared to early trials were indistinguishable (Fig. 3D, G, shown at 110 dB, trial number is not significantly correlated with startle

463 magnitude, Males: controls, r=-0.1950 and *Drd2*$^{Pet1\text{-}CKO}$, r=0.1360. Females: controls,
464 r=0.1171 and *Drd2*$^{Pet1\text{-}CKO}$, r=0.0517, Pearson correlation). Further, we observed no
465 differences in latency to startle in either females or males (Fig. 3E, H). Females were of
466 similar mass (controls: 32.117 ± 3.15 grams vs. *Drd2*$^{Pet1\text{-}CKO}$: 37.2 ± 2.427, unpaired T-
467 test, p=0.2031) regardless of genotype, thus differences in weight and its relative impact
468 on transduction of the startle response via the piezoelectric platform were not a
469 confound.

470 While *Drd2*$^{Pet1\text{-}CKO}$ females showed diminished response magnitudes to startling
471 acoustic stimuli, they nevertheless expressed normal acoustic prepulse inhibition (PPI)
472 whereby even the diminished response to startling acoustic stimuli (e.g. 120 dB stimuli)
473 was further blunted proportionately when immediately preceded by a weak, non-startling
474 stimulus (e.g. 65, 75, or 85 dB stimuli) (Fig. 3I, J). Thus, sensorimotor gating, as
475 measured by acoustic PPI, appeared relatively intact; the acoustic dysfunction instead
476 centered on the ASR itself.

477 Having observed attenuation of the ASR in female *Drd2*$^{Pet1\text{-}CKO}$ mice, we
478 assessed if hearing was broadly disrupted as revealed by auditory brainstem activity
479 responses (ABRs) evoked by sound stimuli (Zhou et al., 2006). ABRs were recorded in
480 response to pure tone stimuli at 5.6, 8, 16, and 32 kHz (n=8 control females, 7 *Drd2*$^{Pet1\text{-}CKO}$
481 females and 10 control males, 7 *Drd2*$^{Pet1\text{-}CKO}$ males). Across all these frequencies,
482 the measured ABR waveforms (Fig. 4A-B, averaged ABR waveforms shown at 16 kHz
483 at 80 dB SPL), peak amplitudes (Fig. 4C, F; shown for peaks 1-3 at 16 kHz at 80 dB
484 SPL for males [p=0.2032, Two-way ANOVA] and females [p=0.1387, Two-way
485 ANOVA]), and latencies to peaks (Fig. 4D, G; shown for peaks 1-3 at 16 kHz at 80 dB

SPL for males [p=0.0804, Two-way ANOVA] and females [p=0.9430, Two-way ANOVA]) were indistinguishable between *Drd2*$^{Pet1\text{-}CKO}$ mice and littermate controls. As well, the ABR threshold to elicit a waveform was not significantly different between *Drd2*$^{Pet1\text{-}CKO}$ and control mice at 5.6, 8, 16 or 32 kHz ($p>0.05$ at all frequencies, unpaired t-test) in males (Fig. 4E) or females (Fig. 4H). Thus, hearing overall, as measured by ABR, appeared largely unaffected in *Drd2*$^{Pet1\text{-}CKO}$ mice.

ABRs were conducted in adult mice (ages P71-102) to align with the age at which the other behavioral assays were performed. However at such ages, C57BL/6 mice – the strain background here – exhibit some age-related hearing loss at higher frequencies (Kane et al., 2012), which we saw here at 32 kHz with two control and three *Drd2*$^{Pet1\text{-}CKO}$ females and five control and three *Drd2*$^{Pet1\text{-}CKO}$males. At all other tested frequencies, the ABRs were effectively normal for both genotypes, with one exception being a *Drd2*$^{Pet1\text{-}CKO}$ female that exhibited undetectable ABRs at 5.6 kHz, but otherwise normal responses at all other frequencies tested including 32 kHz. These findings at 32 and 5.6 kHz are likely independent of the ASR phenotype observed in females because all animals had normal hearing at 8 and 16 kHz – frequencies included in the white noise startle stimulus of the ASR test.

Next, we examined social behavior in *Drd2*$^{Pet1\text{-}CKO}$ mice using the three-chambered test of sociability (Moy et al., 2004) that measures preference to investigate a social stimulus (a novel 'stranger' mouse inside a holder) as compared to an object (an empty holder). *Drd2*$^{Pet1\text{-}CKO}$ mice showed no alterations in sociability compared to controls and both control and *Drd2*$^{Pet1\text{-}CKO}$ spent significantly more time investigating the 'stranger' than the object (Fig. 5A-B). Females of both genotypes displayed preference

towards the social stimuli only for the first five minutes of the assay (Fig. 5B, white bars), while males displayed this preference throughout the ten-minute assay. Similar sex differences in sustained preference for the social stimulus have been described in C57BL/6J mice (Netser et al., 2017)

We assayed intermale, territorial aggression in a separate cohort of mice using a resident intruder assay. Females were not tested, as they have been shown to display low or no aggression in most forms of this assay (Palanza, 2001; Lonstein and Gammie, 2002). We observed no statistically significant difference in number of attack bites delivered to the intruder mouse by *Drd2*$^{Pet1\text{-}CKO}$ males (n=26) compared to number of attack bites delivered to the intruder by controls (n=24) (Fig. 5C, *Drd2*$^{Pet1\text{-}CKO}$: 4.07 ± 1.50 bites, controls: 1.77 ± 0.39 bites, p=0.6649, Mann-Whitney Test) noting though that four *Drd2*$^{Pet1\text{-}CKO}$ males displayed high levels of aggression.

To assay social dominance, we performed the tube test, which has relevance in females as well as males (Lindzey et al., 1961; van den Berg et al., 2015; Zhou et al., 2017). Two mice are simultaneously released into opposite ends of a clear tube of sufficiently narrow diameter that prevents mice from passing by each other and instead requires that one back out for the other, more dominant “winning” mouse, to move forward (Fig. 5D). *Drd2*$^{Pet1\text{-}CKO}$ males won a higher percentage of trials against non-sibling, weight- and genetic background-matched opponent males (Fig. 5E, shown as percent of trials won, *Drd2*$^{Pet1\text{-}CKO}$: 65.83% ± 9, n=24; controls: 34.17% ± 9, n=24; p=0.0065, Mann-Whitney Test). By contrast, we observed no difference in percent of trials won by female *Drd2*$^{Pet1\text{-}CKO}$ mice as compared to female sibling controls (Fig. 5E,

531 *Drd2*$^{Pet1\text{-}CKO}$: 48.7% ± 8, n=23; controls 51.3% ± 8, n=23; p=0.8123, Mann-Whitney
532 Test).

533 ***Drd2-Pet1* neurons in males versus females exhibit differences in candidate**
534 **molecular and biophysical properties but not in cell number**

535 Given these sex-specific differences in behaviors observed in *Drd2*$^{Pet1\text{-}CKO}$ mice,
536 next we looked for sex-specific differences in *Drd2-Pet1* cellular properties, beginning
537 with cell number. Analyzing triple transgenic *Drd2-cre; Pet1-Flpe; RC-FrePe* males
538 versus females, we found no difference in number of GFP^{+} *Drd2-Pet1* neurons per brain
539 (Fig. 6A. Males: 410.40 ± 55.30 cells/brain, Females: 313 ± 87.52 cells/brain, p=0.4304,
540 unpaired T-test). Further, in both males and females, *Drd2-Pet1* neurons distributed as
541 expected across the rostral-caudal and medial-lateral axis of the DR.

542 To understand if gene expression might differ between male and female *Drd2-*
543 *Pet1* neurons, we examined single-cell RNA sequencing data previously analyzed for
544 expression of serotonergic pathway genes as validation that *Drd2-Pet1* cells were
545 indeed serotonergic (Niederkofler et al., 2016). Comparison across sex, albeit lacking
546 statistical significance given the small sample size, highlighted four genes for further
547 evaluation – *Drd2, Dmd* (encoding Dystrophin, a component of protein scaffolds in the
548 CNS (Perronnet and Vaillend, 2010)), *Gad2* (encoding glutamate decarboxylase 2
549 involved in catalyzing the production of the neurotransmitter gamma aminobutyric acid
550 (GABA)), and *Serpini1* (encoding the serine protease Neuroserpin, important for
551 synapse formation and plasticity (Galliciotti and Sonderegger, 2006)). Quantitative in
552 situ mRNA detection using dual fluorescent *in situ* hybridization with immunodetection
553 on tissue sections from *Drd2-Cre;Pet1-Flpe;RC-FrePe* mice revealed greater

abundance of average *Gad2* transcripts (puncta) per cell in males versus females (Fig. 6D; *Gad2*: 20.46 ± 2.243 in males (n=5) versus 12.20 ± 2.427 in females (n=5), p=0.0370, unpaired T-test). There was no difference in the percentage of *Drd2-Pet1* neurons expressing *Gad2* in male versus female mice (Fig. 6E). No difference in soma size (GFP-stained cell body) was observed between males and females suggesting that transcript differences were not due to larger soma volume measured (Fig. 6C). No significant differences in mRNA abundance were observed between males and females for *Dmd*, *Drd2,* or *Serpini1* (see Table 2).

As a first step towards understanding if sex-specific gene expression differences observed in wild-type mice persist or are altered in $Drd2^{Pet1\text{-CKO}}$ mice, we assessed *Gad2* transcript levels in $Drd2^{Pet1\text{-CKO}}$ cells. In these cells, the floxed exon 2 of *Drd2* is excised by Cre recombination. Therefore, to identify mutant *Drd2* mRNA and thus the mutant $Drd2^{Pet1\text{-CKO}}$ cells, we used a multi-probe strategy involving one probe to intact downstream exons 7 and 8 (referred to here as *Drd2*-E7/8*),* another to exon 2 (referred to as *Drd2*-E2), and another to either *cre* or *Pet1*. We examined expression in the DR region most enriched with *Drd2-Pet1* neurons. We found *Drd2*-E7/8+ puncta in *Pet1+* cells in both controls and $Drd2^{Pet1\text{-CKO}}$ mice, whereas *Drd2*-E2+ puncta were detectable in control tissue but greatly reduced in $Drd2^{Pet1\text{-CKO}}$ as expected given the efficiency of Cre-mediated gene deletion (Fig. 7A, see *Drd2*-E2 quantification in Fig. 1E). *Drd2*-E7/8 puncta were detected in 35.97 ± 2.403% of *Pet1+* cells in control mice (n=6) compared to 36.53% ± 3.621 of *Pet1+* cells in $Drd2^{Pet1\text{-CKO}}$ mice (n=6) (p=0.8998, unpaired T-test) (Fig. 7B). Similarly, in a separate experiment using an *in situ* probe to *cre* mRNA*,* 34.91% ± 2.238 of *cre+* cells expressed *Drd2*-E7/8 (n=10 mice, one-way ANOVA

compared to *Pet1* control and *Drd2*$^{Pet1\text{-}CKO}$ cell expression, p= 0.9051) (Fig. 7B). Next, we analyzed *Gad2* mRNA transcript levels in *Drd2*$^{Pet1\text{-}CKO}$ cells (dual *Drd2*-E7/8+ and *cre*+ cells) in the DR (Fig. 7C). In males, we observed 87.44% ± 3.034 of *Drd2*$^{Pet1\text{-}CKO}$ cells were *Gad2*+, while this percentage was 75.76 ± 0.5862% in females (Fig. 7D, p=0.0157, unpaired T-test). In these *Drd2*$^{Pet1\text{-}CKO}$ cells, there were 14.25 ± 1.325 transcripts per cell in males and 10.13 ± 2.074 transcripts per cell in females (Fig. 7E. p=0.1151, unpaired T-test). Due to the tightly packed distribution of cells in the DR, puncta were measured only within *cre*+ DAPI-stained nuclei to ensure puncta were not assigned to more than one cell. The area of nuclei did not differ between males (114.9 ± 3.030 μm^2) and females (Fig. 7F. 110.9 ± 1.768 μm^2, p=0.3497, unpaired T-test). Thus, in *Drd2*$^{Pet1\text{-}CKO}$ males as compared to *Drd2*$^{Pet1\text{-}CKO}$ females, a greater percentage of the *Drd2-Pet1* cells harbored *Gad2* transcripts; of these *Gad2*-expressing cells, however, transcript levels were not significantly different between males versus female *Drd2*$^{Pet1\text{-}CKO}$ mice.

To explore potential sex differences in electrophysiological properties characterizing *Drd2-Pet1* neurons, we conducted whole-cell recordings from GFP-labeled *Drd2-Pet1* neurons in brain slices from triple transgenic *Drd2-Cre;Pet1-Flpe;RC-FrePe* males and females. Examination of cell membrane characteristics revealed no sex differences in resting membrane potential (AP) (Fig. 8A) or resistance (Fig. 8B). Analyses of action potential (AP) characteristics revealed an increase in AP duration (Fig. 8E) in male *Drd2-Pet1* cells as compared to female (2.847 ms ± 0.155, n=19 cells versus 2.54 ms ± 0.094, n=44 cells, respectively, p=0.0275, unpaired T-test), but no

differences in AP threshold (Fig. 8C), amplitude (Fig. 8D), or afterhyperpolarization (AHP) amplitude (Fig. 8F).

Differing covariance in axonal collateral densities from *Drd2-Pet1* neurons directed to auditory targets in males versus females

As a first step in exploring sex differences in *Drd2-Pet1* neuron circuitry that may underlie the sex-specific behavioral phenotypes in $Drd2^{Pet1\text{-}CKO}$ mice, we compared relative innervation density to brain regions involved in sensory processing and social behavior in male and female mice. Boutons from *Drd2-Pet1* neurons were selectively marked with a Synaptophysin-GFP fusion protein using triple transgenic *Drd2-Cre*, *Pet1-Flpe, RC-FPSit* mice (Fig. 9A-B) (Niederkofler et al., 2016). At P90, the same age at which the behavioral assays were conducted, we collected brain tissue and quantified projections to the cochlear nucleus complex (CNC), superior olivary complex (SOC), lateral lemniscus (LL), inferior colliculus (IC), caudal pontine reticular nucleus (PNC, critical for ASR (Davis et al., 1982)), dorsal lateral geniculate nucleus (dLGN), medial preoptic area (mPOA), medial habenula (mHb), periaqueductal gray (PAG), and dorsal paragigantocellular nucleus (DPGi) (Fig. 9C, shown as percentage of target area occupied by projections). We observed no significant sex differences in the cohort average for absolute innervation density to each of these 10 brain regions. However, because we observed considerable inter-animal variability in bouton densities at targets, we next explored correlation of innervation density across brain regions (Weissbourd et al., 2014). Using pairwise correlations between auditory brain regions (Fig. 9D), we constructed a correlation matrix that shows positively correlated regions in green and negatively correlated regions in black (Fig. 9E). This visualization reveals that most

auditory brain regions are positively correlated in males (SOC and LL, Pearson's r=0.89) with only the lateral lemniscus and cochlear nucleus being slightly negatively correlated (Pearson's r=- 0.28). Interestingly, a greater number of innervated regions were negatively correlated in females, including the CNC with both the SOC and the IC (r=-0.68 and r=-0.75 respectively), as well as PNC and IC (r=-0.67). The innervation of the PNC and SOC was significantly negatively correlated (r=-0.85, p=0.033, two-tailed test). Further, we expanded analyses to include the dLGN, a region critical for visually-cued potentiation of the acoustic startle (Tischler and Davis, 1983), and found that in females innervation of the dLGN was not strongly correlated with innervation of auditory brain regions, while in males this dLGN innervation was highly negatively correlated with both the SOC (r=-0.91, p=0.033, two-tailed test) and the IC (r=-0.91, p=0.034 , two-tailed test), indicating that *Drd2-Pet1* neuron circuitry may be set up to modulate multisensory information differently in males compared to females.

GABA and 5-HT in *Drd2-Pet1* neurons

Given detection of *Gad2* mRNA in *Drd2-Pet1* neurons, we probed for GABA versus 5-HT immunopositivity in cell soma versus axonal boutons in males versus females. Punctate GABA immunostaining was indeed detectable in some *Drd2-Pet1* neuron soma (Fig. 10A) in both males and females. Yet, in all target brain regions examined, GABA was undetectable in the GFP-marked *Drd2-Pet1* boutons. Shown are representative images from the SOC (Fig. 10B) and IC (Fig. 10C), noting a GABA-positive cell body in the IC (boxed) and GABA-positive staining in the corpus callosum serving as a positive control for GABA immunodetection (Fig. 10D). By contrast, 5-HT

644 immunostaining in *Drd2-Pet1* boutons was readily detectable (Fig. 10B, representative
645 images from the SOC and IC).
646
647 **Discussion**
648 **Strategy**
649 We hypothesized that loss of *Drd2* gene expression and associated DRD2
650 signaling normally observed in certain DR *Pet1*$^{+}$ serotonergic neurons (*Drd2-Pet1*
651 neurons) could impair sensory, social, and/or defensive behaviors. We used the
652 transgenic driver e*Pet-cre* to delete functionally critical *Drd2* gene sequences selectively
653 in serotonergic neurons, thereby abolishing transcript and DRD2 protein function, which
654 would normally initiate in *Pet1* cells during adolescence. We validated these *Drd2*$^{Pet1\text{-}CKO}$
655 mice and examined behavioral responses. Further, we explored *Drd2-Pet1* neurons
656 themselves.
657 **Main Findings**
658 Key findings include the following: (1) Sex-specific behavioral alterations were
659 observed in *Drd2*$^{Pet1\text{-}CKO}$ mice. Females showed a dramatic diminution in the protective,
660 defensive ASR as compared to *Drd2*$^{flox/flox}$ controls, while no differences were observed
661 in males. (2) *Drd2*$^{Pet1\text{-}CKO}$ males, but not females, showed increased winning in the tube
662 test of social dominance against sex- and age-matched controls. (3) No differences
663 were observed in auditory brainstem responses, in prepulse inhibition of acoustic
664 startle, locomotion, cognition, nor various affective behaviors. (4) No sex-specific
665 differences were found in *Drd2-Pet1* neuron number, soma distribution, nor in the set of
666 efferent targets; however, within-animal correlations between efferent densities across

target brain regions suggest differences by sex, thus hinting at sex-specific structural differences in *Drd2-Pet1* neuronal circuitry. (5) *Drd2-Pet1* cells in males as compared to females showed longer action potential durations and higher levels of *Gad2* transcripts (important for GABA synthesis); $Drd2^{Pet1\text{-}CKO}$ cells did not show a sex specific difference in *Gad2* transcript levels, but the percentage of *Drd2-Pet1* cells that were $Gad2^{+}$ in $Drd2^{Pet1\text{-}CKO}$ males was slightly higher than in $Drd2^{Pet1\text{-}CKO}$ females. These findings, coupled with our prior work (Niederkofler et al., 2016) implicating *Drd2-Pet1* neurons in setting levels of defensive aggressive and exploratory behaviors in male mice, suggest that *Drd2-Pet1* neurons may serve as a specialized neuromodulatory interface whereby DRD2 signaling alters serotonergic neuronal activity to shape defensive, protective, and dominance behaviors in a sex-specific manner.

Protective acoustic startle reflex diminished in $Drd2^{Pet1\text{-}CKO}$ females

Defensive posturing in millisecond response to abrupt noise, be it predator or other potential hazard, is a crucial evolutionarily conserved protective mechanism. Loss or blunting of this reflex can result in life-threatening exposure, while excessive enhancement can drive unnecessary, debilitating responses that preclude normal functioning. Thus “tuning” of the ASR setpoint to social and environmental circumstances is likely critical for species survival and well-being. The observed ASR attenuation in female $Drd2^{Pet1\text{-}CKO}$ mice suggests that *Drd2-Pet1* neurons and the regulation of their activity cell autonomously by DRD2 comprises a critical modulatory node for ASR in females. Further, this node appears separate functionally from that involved in acoustic sensorimotor gating, given that acoustic PPI appeared intact in $Drd2^{Pet1\text{-}CKO}$ females, and from hearing, given that ABRs were indistinguishable from

690 controls. Thus, DRD2 signaling in *Drd2-Pet1* neurons forms a functional circuit node
691 specialized in female mice to influence startle to acoustic stimuli.

692 In rats, reduction of 5-HT through synthesis inhibition increases ASR in females,
693 but not males (Pettersson et al., 2016). Predicted reciprocally is that elevated 5-HT
694 levels might blunt ASR in females. Relating this to our findings, it is possible that *Drd2-*
695 *Pet1* neurons are more excitable in the absence of DRD2-mediated inhibition, resulting
696 in increased 5-HT release, perhaps explaining the observed ASR blunting. In wild-type
697 mice, this would predict that under conditions of DA elevation, for example through local
698 DR DA neuron activity associated with arousal and vigilance (Cho et al., 2017), *Drd2-*
699 *Pet1* neuron activity would be inhibited, reducing 5-HT release and thereby tuning a
700 more sensitive ASR, conferring a protective advantage.

701 The ASR circuit follows from cochlea to CN to PNC to spinal motoneurons (Davis
702 et al., 1982; Koch et al., 1992), and receives inputs from auditory centers such as the
703 SOC, IC, and SC (Lauer et al., 2017). *Drd2-Pet1* neurons innervate each of these areas
704 and the PNC, and thus may impart modulation at multiple levels.

705 **Tube test wins increased in *Drd2*$^{Pet1\text{-}CKO}$ males**

706 The increased winning by *Drd2*$^{Pet1\text{-}CKO}$ males in the tube test suggests that loss
707 of DRD2 results in an increase in or favoring of dominance behaviors, at least under
708 these forced, one-on-one interaction conditions. We did not observe significant
709 differences in levels of aggressive attack behaviors by *Drd2*$^{Pet1\text{-}CKO}$ males in a resident-
710 intruder assay. Together these findings suggest that in wild-type mice, DRD2 signaling
711 in *Drd2-Pet1* neurons contributes to tempering certain dominance behaviors under
712 particular conditions.

Understanding how the present results align with our prior work remains a pursuit. In earlier studies using a resident-intruder assay, we observed an increase in various aggressive behaviors in mice in which *Drd2-Pet1* neurons were constitutively silenced, which suggested to us that *Drd2-Pet1* neuron excitation and neurotransmitter release would normally temper such behaviors (i.e. favor non-confrontational, even submissive behaviors). Because canonical DRD2 signaling is inhibitory and, as well, appears largely inhibitory in *Drd2-Pet1* neurons in slice, we predicted that loss of DRD2 signaling would enhance *Drd2-Pet1* cell excitability and neurotransmitter release probability, and thus would suppress or at least not enhance dominance behaviors. Yet $Drd2^{Pet1\text{-}CKO}$ males exhibited enhanced winning in the tube test. Perhaps DRD2 signaling in *Drd2-Pet1* neurons results in cellular activity changes that ultimately lead to a tempering of one-on-one social dominance under some conditions, while extreme, constitutive *Drd2-Pet1* neuron silencing is required to prompt the opposite, in the form of aggression escalation to an intruder. Indeed, other findings also support this notion that dominance by tube test does not necessarily correlate with aggression in a resident-intruder assay (Tammimaki et al., 2010). Differences might also be explained by whether the input conditions trigger *Drd2-Pet1* neurons to release 5-HT versus GABA, should the latter prove a capability, noting that *Drd2-Pet1* cells express *Gad2,* albeit we were unable to show GABA in *Drd2-Pet1* boutons, only their soma.

Interestingly, a subset of $Drd2^{Pet1\text{-}CKO}$ males (4 out of 26) did display increased levels of aggressive behaviors as compared to other $Drd2^{Pet1\text{-}CKO}$ mice and controls, suggesting there may be other influencing variables, yet unknown. This is plausible given that mice deficient for the long isoform of DRD2 ($D_{2L}R$) are reported to show

anxiety- and depressive-like behaviors only following a stress-exposure paradigm (Shioda et al., 2019). Moreover, these stress-induced affective phenotypes in $D_{2L}R$ knock-out mice were abrogated by driving $D_{2L}R$ expression in DR *Pet1*+ serotonergic neurons (Shioda et al., 2019). Together these findings suggest that the behavioral role of *Drd2* expression in *Drd2-Pet1* neurons may be influenced by environmental factors.

Sex specific differences in *Drd2-Pet1* neuron properties

The observed sex-specific differences in *Gad2* transcript levels in *Drd2-Pet1* neurons may contribute to the sex-specific behavioral alterations exhibited by $Drd2^{Pet1\text{-}CKO}$ mice. *Gad2* expression in *Drd2-Pet1* neurons is in line with prior reports showing *Gad2* expression more generally in the serotonergic DR (Nanopoulos et al., 1982; Calizo et al., 2011; Shikanai et al., 2012). It may be that *Drd2-Pet1* neurons can release GABA as well as or instead of 5-HT under certain conditions or at particular targets. This capacity may differ in males versus females, given our observation that in males, *Drd2-Pet1* neurons harbor higher levels of *Gad2* mRNA. Interestingly, $Drd2^{Pet1\text{-}CKO}$ cells did not display this sex specific difference in *Gad2* transcript, suggesting that *Drd2* expression, or more broadly dopaminergic signaling in *Drd2-Pet1* neurons, may affect *Gad2* transcript levels. One potential model to be tested is if DRD2 signaling, in turn, alters levels of *Gad2* expression to allow for neuronal release of GABA in addition to or instead of serotonin when behavioral or environmental conditions necessitate. Indeed, there is precedent for the differential usage of serotonin and glutamate by raphe serotonergic neurons (Liu et al., 2014; Kapoor et al., 2016; Sengupta et al., 2017; Wang et al., 2019) though GABAergic and serotonergic co-release has not been reported.

Action potential duration measured *ex vivo* was longer in male versus female *Drd2-Pet1* cells; this may also confer neurotransmitter release properties that could contribute to behavioral differences. Additional studies are needed to determine how *Drd2*$^{Pet1\text{-}CKO}$ affects *Drd2-Pet1* neuron electrophysiology, gene expression, or efferent targets. Such experiments may be achieved through crossing *Drd2*$^{Pet1\text{-}CKO}$ *(ePet1-Cre;Drd2*$^{f/f}$*)* mice to *Drd2-Flpo* mice (Jackson labs #034419) along with an intersectional reporter transgene which would allow for dual Cre- and Flp-mediated fluorescent labeling of mutant *Drd2*$^{Pet1\text{-}CKO}$ cells. While complex genetics, this strategy would enable mutant cell visualization for electrophysiology, single-cell RNA sequencing, and analysis of axonal projections.

In both males and females, *Drd2-Pet1* neurons densely innervate auditory brainstem regions, likely modulating auditory-related processes at one or multiple of these sites. In examining *Drd2-Pet1* efferents, we observed inter-animal variability in regional innervation density. We speculated this may arise from subgroups within the *Drd2-Pet1* neuron population that target different downstream structures. For example, some *Drd2-Pet1* neurons may project specifically to the SOC while others might project specifically to the LL. If some animals have more of one subgroup than the other, averaging absolute innervation densities for each target region across all males and females may hide meaningful circuit structure. Covariance analysis of projection targets in each animal thus might hint at which brain regions come under shared regulation by *Drd2-Pet1* neurons. In males, the high correlation between auditory region efferent densities suggests shared input from the same *Drd2-Pet1* neurons. In females, the CNC/SOC, CNC/IC, SOC/PNC, LL/PNC, and IC/PNC combinations were more

781 negatively correlated, suggesting there might exist a subgroup of *Drd2-Pet1* neurons
782 that targets the PNC and a different subgroup, the SOC. We speculate that in males,
783 *Drd2-Pet1* neurons contribute to a general level of serotonergic tone across the auditory
784 brainstem, while in females, certain *Drd2-Pet1* neurons selectively target and modulate
785 specific nuclei.

786 In conclusion, we found that *Drd2* gene expression in a specialized subset of
787 *Pet1* serotonergic neurons is required for certain defensive, dominance, and protective
788 behaviors, involving auditory processing in a sex-specific manner. Deficits in sensory
789 processing such as altered acoustic startle and impaired social communication and
790 dominance behaviors manifest in human disorders including autism spectrum disorder,
791 schizophrenia, and post-traumatic stress disorder, often in sex-specific ways (King et
792 al., 2013; Steel et al., 2014; Matsuo et al., 2016; Thye et al., 2018) and with sex-specific
793 differences in therapeutic outcomes (Franconi et al., 2007). The presented findings,
794 thus, may point to novel circuit nodes of relevance to human neuropsychiatric disease.

795 **References**

796 Baik, J. H., Picetti, R., Saiardi, A., Thiriet, G., Dierich, A., Depaulis, A., Le Meur, M., and
797 Borrelli, E. (1995). Parkinsonian-like locomotor impairment in mice lacking dopamine D2
798 receptors. Nature *377*, 424-428.
799 Bello, E. P., Mateo, Y., Gelman, D. M., Noain, D., Shin, J. H., Low, M. J., Alvarez, V. A.,
800 Lovinger, D. M., and Rubinstein, M. (2011). Cocaine supersensitivity and enhanced
801 motivation for reward in mice lacking dopamine D2 autoreceptors. Nat Neurosci *14*,
802 1033-1038.

803 Brown, G. L., Ebert, M. H., Goyer, P. F., Jimerson, D. C., Klein, W. J., Bunney, W. E.,
804 and Goodwin, F. K. (1982). Aggression, suicide, and serotonin: relationships to CSF
805 amine metabolites. Am J Psychiatry *139*, 741-746.
806 Brust, R. D., Corcoran, A. E., Richerson, G. B., Nattie, E., and Dymecki, S. M. (2014).
807 Functional and developmental identification of a molecular subtype of brain serotonergic
808 neuron specialized to regulate breathing dynamics. Cell Rep *9*, 2152-2165.
809 Calizo, L. H., Akanwa, A., Ma, X., Pan, Y. Z., Lemos, J. C., Craige, C., Heemstra, L. A.,
810 and Beck, S. G. (2011). Raphe serotonin neurons are not homogenous:
811 electrophysiological, morphological and neurochemical evidence. Neuropharmacology
812 *61*, 524-543.
813 Cho, J. R., Treweek, J. B., Robinson, J. E., Xiao, C., Bremner, L. R., Greenbaum, A.,
814 and Gradinaru, V. (2017). Dorsal Raphe Dopamine Neurons Modulate Arousal and
815 Promote Wakefulness by Salient Stimuli. Neuron *94*, 1205-1219 e1208.
816 Crawford, L. K., Rahman, S. F., and Beck, S. G. (2013). Social stress alters inhibitory
817 synaptic input to distinct subpopulations of raphe serotonin neurons. ACS Chem
818 Neurosci *4*, 200-209.
819 Davis, M., and Aghajanian, G. K. (1976). Effects of apomorphine and haloperidol on the
820 acoustic startle response in rats. Psychopharmacology (Berl) *47*, 217-223.
821 Davis, M., Gendelman, D. S., Tischler, M. D., and Gendelman, P. M. (1982). A primary
822 acoustic startle circuit: lesion and stimulation studies. J Neurosci *2*, 791-805.
823 Davis, M., Strachan, D. I., and Kass, E. (1980). Excitatory and inhibitory effects of
824 serotonin on sensorimotor reactivity measured with acoustic startle. Science *209*, 521-
825 523.

826 Deneris, E., and Gaspar, P. (2018). Serotonin neuron development: shaping molecular
827 and structural identities. Wiley Interdiscip Rev Dev Biol *7*.
828 Franconi, F., Brunelleschi, S., Steardo, L., and Cuomo, V. (2007). Gender differences in
829 drug responses. Pharmacol Res *55*, 81-95.
830 Franklin, K. B. J., and Paxinos, G. (2008). The Mouse Brain in Stereotaxic Coordinates
831 Vol 3, (New Yotk: Elsevier).
832 Gainetdinov, R. R., Wetsel, W. C., Jones, S. R., Levin, E. D., Jaber, M., and Caron, M.
833 G. (1999). Role of serotonin in the paradoxical calming effect of psychostimulants on
834 hyperactivity. Science *283*, 397-401.
835 Galliciotti, G., and Sonderegger, P. (2006). Neuroserpin. Front Biosci *11*, 33-45.
836 Geyer, M. A., and Braff, D. L. (1987). Startle habituation and sensorimotor gating in
837 schizophrenia and related animal models. Schizophr Bull *13*, 643-668.
838 Gong, S., Doughty, M., Harbaugh, C. R., Cummins, A., Hatten, M. E., Heintz, N., and
839 Gerfen, C. R. (2007). Targeting Cre recombinase to specific neuron populations with
840 bacterial artificial chromosome constructs. J Neurosci *27*, 9817-9823.
841 Grace, A. A. (2016). Dysregulation of the dopamine system in the pathophysiology of
842 schizophrenia and depression. Nat Rev Neurosci *17*, 524-532.
843 Hendricks, T. J., Fyodorov, D. V., Wegman, L. J., Lelutiu, N. B., Pehek, E. A.,
844 Yamamoto, B., Silver, J., Weeber, E. J., Sweatt, J. D., and Deneris, E. S. (2003). Pet-1
845 ETS gene plays a critical role in 5-HT neuron development and is required for normal
846 anxiety-like and aggressive behavior. Neuron *37*, 233-247.

847 Holmes, A., Yang, R. J., Lesch, K. P., Crawley, J. N., and Murphy, D. L. (2003). Mice
848 lacking the serotonin transporter exhibit 5-HT(1A) receptor-mediated abnormalities in
849 tests for anxiety-like behavior. Neuropsychopharmacology *28*, 2077-2088.
850 Holschbach, M. A., Vitale, E. M., and Lonstein, J. S. (2018). Serotonin-specific lesions
851 of the dorsal raphe disrupt maternal aggression and caregiving in postpartum rats.
852 Behav Brain Res *348*, 53-64.
853 Huang, K. W., Ochandarena, N. E., Philson, A. C., Hyun, M., Birnbaum, J. E., Cicconet,
854 M., and Sabatini, B. L. (2019). Molecular and anatomical organization of the dorsal
855 raphe nucleus. Elife *8*.
856 Jensen, P., Farago, A. F., Awatramani, R. B., Scott, M. M., Deneris, E. S., and Dymecki,
857 S. M. (2008). Redefining the serotonergic system by genetic lineage. Nat Neurosci *11*,
858 417-419.
859 Kane, K. L., Longo-Guess, C. M., Gagnon, L. H., Ding, D., Salvi, R. J., and Johnson, K.
860 R. (2012). Genetic background effects on age-related hearing loss associated with
861 Cdh23 variants in mice. Hear Res *283*, 80-88.
862 Kapoor, V., Provost, A. C., Agarwal, P., and Murthy, V. N. (2016). Activation of raphe
863 nuclei triggers rapid and distinct effects on parallel olfactory bulb output channels. Nat
864 Neurosci *19*, 271-282.
865 Kim, J. C., Cook, M. N., Carey, M. R., Shen, C., Regehr, W. G., and Dymecki, S. M.
866 (2009). Linking genetically defined neurons to behavior through a broadly applicable
867 silencing allele. Neuron *63*, 305-315.

King, M. W., Street, A. E., Gradus, J. L., Vogt, D. S., and Resick, P. A. (2013). Gender differences in posttraumatic stress symptoms among OEF/OIF veterans: an item response theory analysis. J Trauma Stress *26*, 175-183.

Koch, M., Lingenhohl, K., and Pilz, P. K. (1992). Loss of the acoustic startle response following neurotoxic lesions of the caudal pontine reticular formation: possible role of giant neurons. Neuroscience *49*, 617-625.

Lammel, S., Lim, B. K., and Malenka, R. C. (2014). Reward and aversion in a heterogeneous midbrain dopamine system. Neuropharmacology *76 Pt B*, 351-359.

Lauer, A. M., Behrens, D., and Klump, G. (2017). Acoustic startle modification as a tool for evaluating auditory function of the mouse: Progress, pitfalls, and potential. Neurosci Biobehav Rev *77*, 194-208.

Lindzey, G., Winston, H., and Manosevitz, M. (1961). Social dominance in inbred mouse strains. Nature *191*, 474-476.

Liu, Z., Zhou, J., Li, Y., Hu, F., Lu, Y., Ma, M., Feng, Q., Zhang, J. E., Wang, D., Zeng, J., Bao, J., Kim, J. Y., Chen, Z. F., El Mestikawy, S., and Luo, M. (2014). Dorsal raphe neurons signal reward through 5-HT and glutamate. Neuron *81*, 1360-1374.

Lonstein, J. S., and Gammie, S. C. (2002). Sensory, hormonal, and neural control of maternal aggression in laboratory rodents. Neurosci Biobehav Rev *26*, 869-888.

Lucki, I. (1998). The spectrum of behaviors influenced by serotonin. Biol Psychiatry *44*, 151-162.

Maison, S. F., Usubuchi, H., and Liberman, M. C. (2013). Efferent feedback minimizes cochlear neuropathy from moderate noise exposure. J Neurosci *33*, 5542-5552.

Marr, D., and Hildreth, E. (1980). Theory of edge detection. Proc R Soc Lond B Biol Sci *207*, 187-217.

Matsuo, J., Ota, M., Hori, H., Hidese, S., Teraishi, T., Ishida, I., Hiraishi, M., and Kunugi, H. (2016). A large single ethnicity study of prepulse inhibition in schizophrenia: Separate analysis by sex focusing on effect of symptoms. J Psychiatr Res *82*, 155-162.

McQuin, C., Goodman, A., Chernyshev, V., Kamentsky, L., Cimini, B. A., Karhohs, K. W., Doan, M., Ding, L., Rafelski, S. M., Thirstrup, D., Wiegraebe, W., Singh, S., Becker, T., Caicedo, J. C., and Carpenter, A. E. (2018). CellProfiler 3.0: Next-generation image processing for biology. PLoS Biol *16*, e2005970.

Meincke, U., Light, G. A., Geyer, M. A., Braff, D. L., and Gouzoulis-Mayfrank, E. (2004). Sensitization and habituation of the acoustic startle reflex in patients with schizophrenia. Psychiatry Res *126*, 51-61.

Meloni, E. G., and Davis, M. (1999). Enhancement of the acoustic startle response in rats by the dopamine D1 receptor agonist SKF 82958. Psychopharmacology (Berl) *144*, 373-380.

Meloni, E. G., and Davis, M. (2000a). Enhancement of the acoustic startle response by dopamine agonists after 6-hydroxydopamine lesions of the substantia nigra pars compacta: corresponding changes in c-Fos expression in the caudate-putamen. Brain Res *879*, 93-104.

Meloni, E. G., and Davis, M. (2000b). Synergistic enhancement of the acoustic startle reflex by dopamine D1 and 5-HT1A agonists and corresponding changes in c-Fos expression in the dorsal raphe of rats. Psychopharmacology (Berl) *151*, 359-367.

912 Moy, S. S., Nadler, J. J., Perez, A., Barbaro, R. P., Johns, J. M., Magnuson, T. R.,
913 Piven, J., and Crawley, J. N. (2004). Sociability and preference for social novelty in five
914 inbred strains: an approach to assess autistic-like behavior in mice. Genes Brain Behav
915 *3*, 287-302.
916 Nanopoulos, D., Belin, M. F., Maitre, M., Vincendon, G., and Pujol, J. F. (1982).
917 Immunocytochemical evidence for the existence of GABAergic neurons in the nucleus
918 raphe dorsalis. Possible existence of neurons containing serotonin and GABA. Brain
919 Res *232*, 375-389.
920 Netser, S., Haskal, S., Magalnik, H., and Wagner, S. (2017). A novel system for tracking
921 social preference dynamics in mice reveals sex- and strain-specific characteristics.
922 Molecular Autism *8*.
923 Niederkofler, V., Asher, T. E., Okaty, B. W., Rood, B. D., Narayan, A., Hwa, L. S., Beck,
924 S. G., Miczek, K. A., and Dymecki, S. M. (2016). Identification of Serotonergic Neuronal
925 Modules that Affect Aggressive Behavior. Cell Rep *17*, 1934-1949.
926 Okaty, B. W., Freret, M. E., Rood, B. D., Brust, R. D., Hennessy, M. L., deBairos, D.,
927 Kim, J. C., Cook, M. N., and Dymecki, S. M. (2015). Multi-Scale Molecular
928 Deconstruction of the Serotonin Neuron System.
929 Okaty, B. W., Sturrock, N., Escobedo Lozoya, Y., Chang, Y., Senft, R. A., Lyon, K. A.,
930 Alekseyenko, O. V., and Dymecki, S. M. (2020). A single-cell transcriptomic and
931 anatomic atlas of mouse dorsal raphe Pet1 neurons. Elife *9*.
932 Palanza, P. (2001). Animal models of anxiety and depression: how are females
933 different? Neurosci Biobehav Rev *25*, 219-233.

934 Perronnet, C., and Vaillend, C. (2010). Dystrophins, utrophins, and associated
935 scaffolding complexes: role in mammalian brain and implications for therapeutic
936 strategies. J Biomed Biotechnol *2010*, 849426.
937 Pettersson, R., Hagsater, S. M., and Eriksson, E. (2016). Serotonin depletion eliminates
938 sex differences with respect to context-conditioned immobility in rat.
939 Psychopharmacology (Berl) *233*, 1513-1521.
940 Poulin, J. F., Caronia, G., Hofer, C., Cui, Q., Helm, B., Ramakrishnan, C., Chan, C. S.,
941 Dombeck, D. A., Deisseroth, K., and Awatramani, R. (2018). Mapping projections of
942 molecularly defined dopamine neuron subtypes using intersectional genetic
943 approaches. Nat Neurosci *21*, 1260-1271.
944 Poulin, J. F., Gaertner, Z., Moreno-Ramos, O. A., and Awatramani, R. (2020).
945 Classification of Midbrain Dopamine Neurons Using Single-Cell Gene Expression
946 Profiling Approaches. Trends Neurosci *43*, 155-169.
947 Ralph, R. J., Paulus, M. P., Fumagalli, F., Caron, M. G., and Geyer, M. A. (2001).
948 Prepulse inhibition deficits and perseverative motor patterns in dopamine transporter
949 knock-out mice: differential effects of D1 and D2 receptor antagonists. J Neurosci *21*,
950 305-313.
951 Ren, J., Isakova, A., Friedmann, D., Zeng, J., Grutzner, S. M., Pun, A., Zhao, G. Q.,
952 Kolluru, S. S., Wang, R., Lin, R., Li, P., Li, A., Raymond, J. L., Luo, Q., Luo, M., Quake,
953 S. R., and Luo, L. (2019). Single-cell transcriptomes and whole-brain projections of
954 serotonin neurons in the mouse dorsal and median raphe nuclei. Elife *8*.
955 Rood, B. D., Calizo, L. H., Piel, D., Spangler, Z. P., Campbell, K., and Beck, S. G.
956 (2014). Dorsal raphe serotonin neurons in mice: immature hyperexcitability transitions to

957 adult state during first three postnatal weeks suggesting sensitive period for
958 environmental perturbation. J Neurosci *34*, 4809-4821.
959 Schindelin, J., Arganda-Carreras, I., Frise, E., Kaynig, V., Longair, M., Pietzsch, T.,
960 Preibisch, S., Rueden, C., Saalfeld, S., Schmid, B., Tinevez, J. Y., White, D. J.,
961 Hartenstein, V., Eliceiri, K., Tomancak, P., and Cardona, A. (2012). Fiji: an open-source
962 platform for biological-image analysis. Nat Methods *9*, 676-682.
963 Scott, M. M., Wylie, C. J., Lerch, J. K., Murphy, R., Lobur, K., Herlitze, S., Jiang, W.,
964 Conlon, R. A., Strowbridge, B. W., and Deneris, E. S. (2005). A genetic approach to
965 access serotonin neurons for in vivo and in vitro studies. Proc Natl Acad Sci U S A *102*,
966 16472-16477.
967 Sengupta, A., Bocchio, M., Bannerman, D. M., Sharp, T., and Capogna, M. (2017).
968 Control of Amygdala Circuits by 5-HT Neurons via 5-HT and Glutamate Cotransmission.
969 J Neurosci *37*, 1785-1796.
970 Seo, C., Guru, A., Jin, M., Ito, B., Sleezer, B. J., Ho, Y. Y., Wang, E., Boada, C., Krupa,
971 N. A., Kullakanda, D. S., Shen, C. X., and Warden, M. R. (2019). Intense threat
972 switches dorsal raphe serotonin neurons to a paradoxical operational mode. Science
973 *363*, 538-542.
974 Shikanai, H., Yoshida, T., Konno, K., Yamasaki, M., Izumi, T., Ohmura, Y., Watanabe,
975 M., and Yoshioka, M. (2012). Distinct neurochemical and functional properties of
976 GAD67-containing 5-HT neurons in the rat dorsal raphe nucleus. J Neurosci *32*, 14415-
977 14426.
978 Shioda, N., Imai, Y., Yabuki, Y., Sugimoto, W., Yamaguchi, K., Wang, Y., Hikida, T.,
979 Sasaoka, T., Mieda, M., and Fukunaga, K. (2019). Dopamine D2L Receptor Deficiency

Causes Stress Vulnerability through 5-HT1A Receptor Dysfunction in Serotonergic Neurons. J Neurosci.

Shrestha, B. R., Chia, C., Wu, L., Kujawa, S. G., Liberman, M. C., and Goodrich, L. V. (2018). Sensory Neuron Diversity in the Inner Ear Is Shaped by Activity. Cell *174*, 1229-1246 e1217.

Spaethling, J. M., Piel, D., Dueck, H., Buckley, P. T., Morris, J. F., Fisher, S. A., Lee, J., Sul, J. Y., Kim, J., Bartfai, T., Beck, S. G., and Eberwine, J. H. (2014). Serotonergic neuron regulation informed by in vivo single-cell transcriptomics. FASEB J *28*, 771-780.

Spannuth, B. M., Hale, M. W., Evans, A. K., Lukkes, J. L., Campeau, S., and Lowry, C. A. (2011). Investigation of a central nucleus of the amygdala/dorsal raphe nucleus serotonergic circuit implicated in fear-potentiated startle. Neuroscience *179*, 104-119.

Steel, Z., Marnane, C., Iranpour, C., Chey, T., Jackson, J. W., Patel, V., and Silove, D. (2014). The global prevalence of common mental disorders: a systematic review and meta-analysis 1980-2013. Int J Epidemiol *43*, 476-493.

Takahashi, H., and Kamio, Y. (2018). Acoustic startle response and its modulation in schizophrenia and autism spectrum disorder in Asian subjects. Schizophr Res *198*, 16-20.

Tammimaki, A., Kaenmaki, M., Kambur, O., Kulesskaya, N., Keisala, T., Karvonen, E., Garcia-Horsman, J. A., Rauvala, H., and Mannisto, P. T. (2010). Effect of S-COMT deficiency on behavior and extracellular brain dopamine concentrations in mice. Psychopharmacology (Berl) *211*, 389-401.

Terranova, J. I., Song, Z., Larkin, T. E., 2nd, Hardcastle, N., Norvelle, A., Riaz, A., and Albers, H. E. (2016). Serotonin and arginine-vasopressin mediate sex differences in the

regulation of dominance and aggression by the social brain. Proc Natl Acad Sci U S A *113*, 13233-13238.

Thye, M. D., Bednarz, H. M., Herringshaw, A. J., Sartin, E. B., and Kana, R. K. (2018). The impact of atypical sensory processing on social impairments in autism spectrum disorder.

Tischler, M. D., and Davis, M. (1983). A visual pathway that mediates fear-conditioned enhancement of acoustic startle. Brain Res *276*, 55-71.

van den Berg, W. E., Lamballais, S., and Kushner, S. A. (2015). Sex-specific mechanism of social hierarchy in mice. Neuropsychopharmacology *40*, 1364-1372.

Wang, H. L., Zhang, S., Qi, J., Wang, H., Cachope, R., Mejias-Aponte, C. A., Gomez, J. A., Mateo-Semidey, G. E., Beaudoin, G. M. J., Paladini, C. A., Cheer, J. F., and Morales, M. (2019). Dorsal Raphe Dual Serotonin-Glutamate Neurons Drive Reward by Establishing Excitatory Synapses on VTA Mesoaccumbens Dopamine Neurons. Cell Rep *26*, 1128-1142 e1127.

Weissbourd, B., Ren, J., DeLoach, K. E., Guenthner, C. J., Miyamichi, K., and Luo, L. (2014). Presynaptic partners of dorsal raphe serotonergic and GABAergic neurons. Neuron *83*, 645-662.

Yu, Q., Teixeira, C. M., Mahadevia, D., Huang, Y., Balsam, D., Mann, J. J., Gingrich, J. A., and Ansorge, M. S. (2014). Dopamine and serotonin signaling during two sensitive developmental periods differentially impact adult aggressive and affective behaviors in mice. Mol Psychiatry *19*, 688-698.

1024 Zhou, T., Zhu, H., Fan, Z., Wang, F., Chen, Y., Liang, H., Yang, Z., Zhang, L., Lin, L.,
1025 Zhan, Y., Wang, Z., and Hu, H. (2017). History of winning remodels thalamo-PFC circuit
1026 to reinforce social dominance. Science *357*, 162-168.
1027 Zhou, X., Jen, P. H., Seburn, K. L., Frankel, W. N., and Zheng, Q. Y. (2006). Auditory
1028 brainstem responses in 10 inbred strains of mice. Brain Res *1091*, 16-26.

1029 **Figure Legends**

1030 **Figure 1. Visualization of *Drd2-Pet1* serotonergic neurons and the loss of *Drd2***
1031 **gene expression in *Drd2*$^{Pet1\text{-}CKO}$ mice. A,** *Drd2-Pet1* neurons are intersectionally
1032 labeled with GFP (green) and *Pet1*-only positive cell bodies labeled with mCherry
1033 (magenta) in a coronal brain section of the dorsal raphe (DR) from a postnatal day
1034 (P)90 triple transgenic *Drd2-Cre;Pet1-Flpe;RC:FrePe* mouse. Scale bars 200 μm. **B**,
1035 Intersectional genetic strategy: expression of *Drd2:Cre and Pet1:Flpe* transgenes
1036 results in dual recombination of intersectional allele, *RC:FrePe,* labeling cells
1037 expressing *Drd2* and *Pet1* with GFP. **C,** Dual immunohistochemistry for GFP (green)
1038 and 5-HT (serotonin, magenta) coupled with fluorescent *in situ* hybridization detection of
1039 *Drd2* mRNA, which shows co-localization of intersectionally labeled *Drd2-Pet1* neuron
1040 cell bodies with 5-HT and *Drd2* mRNA. Scale bars 10 μm. **D,** Strategy for conditional
1041 deletion of *Drd2* in serotonergic neurons (referred to throughout as *Drd2*$^{Pet1\text{-}CKO}$). Cre
1042 recombination excises *Drd2* exon 2 (magenta) producing serotonergic specific (boxed in
1043 green) deletion of *Drd2* gene sequences. **E,** Percentage (mean ± SEM) of *Pet1*+
1044 serotonergic neurons that express *Drd2* in control (n=6) versus *Drd2*$^{Pet1\text{-}CKO}$ (n=6) shows
1045 reduction of *Drd2* expression in *Pet1*+ neurons (controls: 15.23 ± 2.41 *Drd2-Pet1* dual
1046 positive neurons per brain, *Drd2*$^{Pet1\text{-}CKO}$: 3.87 ± 0.73 *Drd2-Pet1* dual positive neurons

per brain, p=0.0011, unpaired T-test). Filled black diamonds represent male mice, open gray circles represent female mice. **F-G**, Fluorescent *in situ* hybridization on (**F**) control and (**G**) *Drd2*$^{Pet1\text{-CKO}}$ tissue. *Drd2* transcripts detected in *Pet1*+ cells in control sections, but not in *Drd2*$^{Pet1\text{-CKO}}$ mice, indicative of loss of *Drd2*. *cre* transcript is not present in control (**F**, far right), but is present in *Drd2*$^{Pet1\text{-CKO}}$ *Pet1* cells, as expected (**G,** far right). *Pet1*, *Drd2*, and *cre* transcript are shown separately in grayscale. Note *Drd2* expression remains in non-*Pet1* cells (arrow). Dotted lines drawn to encircle DAPI nuclei. Scale bars 25μm.

Figure 2. *Drd2*$^{Pet1\text{-CKO}}$ mice are largely behaviorally normal. *Drd2*$^{Pet1\text{-CKO}}$ (blue symbols) mice show behaviors indistinguishable from controls (black symbols) in measures of locomotion: **A-B,** open field test and **C,** rotarod; measures of anxiety-like and depression-like behavior: **D,** elevated plus maze, **E,** tail suspension test, and **F,** forced swim test; or learning and memory: **G,** contextual fear conditioning and **H,** water T maze. n=15 control mice (8 males, 7 females) and 11 *Drd2*$^{Pet1\text{-CKO}}$ (6 males, 5 females), except for C where, n=21 control mice (14 males, 7 females) and 18 *Drd2*$^{Pet1\text{-CKO}}$ (13 males, 5 females). Each symbol represents one animal, error represents SEM. No significant differences (p>0.05) between *Drd2*$^{Pet1\text{-CKO}}$ and controls were observed. No sex-specific (male versus female) phenotypes observed. See methods for assay details and Table 2 for statistical details.

Figure 3. *Drd2*$^{Pet1\text{-CKO}}$ females, but not males, display attenuated acoustic startle responses (ASR). A, Schematic of ASR experimental design. After an initial 5 min acclimation, mice are exposed to 10 blocks of 11 trials of auditory stimuli ranging from 20-120 dB in quasi-randomized order with a 10-20 second inter-trial interval (ITI). **B,**

Schematic of ASR measurement apparatus, mouse is placed in a perforated holding chamber atop transducer platform adjacent to speaker, see methods for detailed description. **C**, **F,** Averaged ASR magnitudes (mean ± SEM) across increasing stimulus intensities in (**C**) male *Drd2*$^{Pet1\text{-}CKO}$ (blue, n=13) and controls (black, n=14), no significant difference, p=0.7745, Two-way ANOVA and (**F**) female *Drd2*$^{Pet1\text{-}CKO}$ (blue, n=15) and controls (black, n=16), *Drd2*$^{Pet1\text{-}CKO}$ females display significantly attenuated ASR, p=0.0011, Two-way ANOVA. **D, G,** Group averaged ASR for 10 trials at 110 dB stimulus in (**D**) males and (**G**) females, demonstrates no habituation to the startle stimulus. X axis numbers refers to trial number out of 110 total trials. **E, H,** No significant differences in latency to startle are observed in (**E**) males, p=0.1319, Two-way ANOVA and (**H**) females, p=0.5452, Two-way ANOVA. **I-J,** No significant differences in paired-pulse inhibition of acoustic startle are observed in (**I**) males (n=8 control, 6 *Drd2*$^{Pet1\text{-}CKO}$), p=0.4325, Two-way ANOVA or **(J)** females (n=7 control, 5 *Drd2*$^{Pet1\text{-}CKO}$), p=0.4380, Two-way ANOVA).

Figure 4. *Drd2*$^{Pet1\text{-}CKO}$ mice show normal auditory responses. A-B, Average ABR waveforms at 16 kHz for (**A**) control (black, n=10) and *Drd2*$^{Pet1\text{-}CKO}$ (blue, n=7) males and (**B**) for control (black, n=8) and *Drd2*$^{Pet1\text{-}CKO}$ (blue, n=7) females. Average is shown by darker lines and shaded area shows SEM. **C,F,** ABR amplitudes for control (black) and *Drd2*$^{Pet1\text{-}CKO}$ (blue) (**C**) male and (**F**) female mice for ABR peaks 1 through 3. No significant difference was observed between control and *Drd2*$^{Pet1\text{-}CKO}$: males, p=0.2032; females, p=0.1387, Two-way ANOVA. **D, F,** Latencies for control (black) and *Drd2*$^{Pet1\text{-}CKO}$ (blue) (**D**) male and (**G**) female mice for ABR peaks 1 through 3. No significant difference was observed between control and *Drd2*$^{Pet1\text{-}CKO}$: males, p=0.0804; females,

p=0.9430, Two-way ANOVA. Amplitudes and latencies shown at 80 dB SPL. **E, H,** ABR thresholds for control (black) and *Drd2*$^{Pet1\text{-CKO}}$ (blue) (**E**) male and (**H**) female mice across frequencies tested (5.6, 8, 16, and 32 kHz). No significant difference was observed between control and *Drd2*$^{Pet1\text{-CKO}}$ mice, p>0.05 at all frequencies, unpaired t-test.

Figure 5. *Drd2*$^{Pet1\text{-CKO}}$ males, but not females, display increased social dominance. **A-B,** Three chambered social interaction assay. No significant difference in time spent investigating a stranger mouse or an empty holder for (**A**) males (n=8 controls compared to 6 *Drd2*$^{Pet1\text{-CKO}}$, p=0.541, unpaired T-test) and (**B**) females (n=7 controls compared to n=5 *Drd2*$^{Pet1\text{-CKO}}$, p=0.358, unpaired T-test). Investigation time is binned into 5 minute intervals where white bars indicate first five minutes of assay and colored bars indicate last five minutes of assay. As expected, mice of both genotypes spent significantly less time investigating the empty holder than the stranger mouse noting that females of both genotypes only did so during the first five minutes of the assay. **C,** Resident intruder assay of aggression. No significant difference in the average attack bites per day delivered to a Swiss Webster intruder mouse was observed between *Drd2*$^{Pet1\text{-CKO}}$ males (n=26, 4.07 ± 1.50 bites) aggression levels were not significantly different from controls (n=24, 1.77 ± 0.39 bites; Mann-Whitney, two-tailed, U=289.5, p=0.6649). **D**, Schematic of tube test, see methods for details of assay. Schematic created with BioRender.com. **E,** *Drd2*$^{Pet1\text{-CKO}}$ males (n=24) demonstrate more dominance behavior than controls (n=24) as they displayed increased winning in the tube test (Controls: 34.17% ± 9 wins, *Drd2*$^{Pet1\text{-CKO}}$: 65.83% ± 9 wins, p=0.0065, Mann-Whitney, two-tailed, U=166). Female *Drd2*$^{Pet1\text{-CKO}}$ (n=23) showed no difference in social

dominance compared to controls (n=23), (Controls: 51.3% ± 8, *Drd2*$^{Pet1\text{-}CKO}$: 48.7% ± 8 wins, p=0.8123 Mann-Whitney, two-tailed, U=253).

Figure 6. **Sex-specific transcript level differences in *Drd2-Pet1* neurons.**

A, Dual immunohistochemistry and fluorescent *in situ* hybridization depicting green GFP+ *Drd2-Pet1* neurons along with transcript puncta in male (top) and female (bottom) brain sections from *Drd2-Cre;Pet1-Flpe;RC-FrePe* mice. *Drd2* (cyan) and *Gad2* (magenta) expression shown together and separately in gray scale. Scale bar 10 μm. **B,** Number of *Drd2-Pet1* neurons (GFP-positive cells in *Drd2-Cre;Pet1-Flpe;RC-FrePE* mice) per animal in males (black diamonds, n=7) and females (open gray circles, n=7) is not significantly different. Males: 410.40 ± 55.30 cells/brain, Females: 313 ± 87.52 cells/brain, p=0.4336, unpaired T-test. **C,** *Drd2-Pet1* neuron soma size (GFP+ cell body) does not differ in males (n=5 males) versus females (n=5 females), p=0.3372, unpaired T-test. **D,** Number of fluorescent *in situ* hybridization mRNA puncta per cell in males versus females. Male cells have significantly more *Gad2* puncta than female cells (20.46 ± 2.243 in males (n=5) versus 12.20 ± 2.427 in females (n=5), p=0.0370, unpaired T-test. **E,** 86.47% ± 4.181 of male *Drd2-Pet1* cells express *Gad2* versus female 74.00% ± 5.168 in female cells, p=0.0975, unpaired T-test. Error bars indicate SEM throughout. For C and D, larger symbols outlined in black represent animal averages used for statistical analysis, smaller symbols represent individual cells, matched in color to the average.

Figure 7. *Gad2* expression in *Drd2*$^{Pet1\text{-}CKO}$ cells

A, Fluorescent *in situ* hybridization with probes to *Drd2* exon 7/8 (*D2*-E7/8, green) and *Drd2* exon 2 (*D2*-E2, magenta) in *Pet1* (white) cells in control (top) and *Drd2*$^{Pet1\text{-}CKO}$

(bottom) dorsal raphe tissue. *D2*-E7/8, *D2*-E2, and *Pet1* expression shown together and separately in gray scale. **B,** Percent of *Pet1*+ cells (left and middle) with *Drd2*-Exon7/8 expression in control (35.97% ± 2.403, n=6) and $Drd2^{Pet1\text{-}CKO}$ (36.53% ± 3.621, n=6), p=0.8998, unpaired T-test. Data also shown for percent of *cre* cells (right) with *Drd2*-Exon7/8, 34.91% ± 2.238, compared to *Pet1* probe control and $Drd2^{Pet1\text{-}CKO}$ p=0.9051, One-way ANOVA. Males, black diamonds, females, open grey circles. **C,** Fluorescent *in situ* hybridization showing *cre*+ $Drd2^{Pet1\text{-}CKO}$ cells (white) with *Drd2-Exon7/8* (green) *and Gad2* (red) in male (top) and female (bottom) in the dorsal raphe nucleus. *Drd2-Exon7/8, Gad2*, and *cre* are shown together and separately in gray scale. Scale bar 10 µm. **D,** A larger percentage of male $Drd2^{Pet1\text{-}CKO}$ cells (87.44% ± 3.034) express *Gad2* versus female $Drd2^{Pet1\text{-}CKO}$ cells (75.76% ± 0.5862), *p=0.0157, unpaired T-test. **E,** Number of *Gad2* mRNA puncta per cell in $Drd2^{Pet1\text{-}CKO}$ cells in males (n=6) versus females (n=4). Male cells have 14.25 ± 1.325 *Gad2* puncta per cell compared to 10.13 ± 2.074 in female cells, p=0.1151, unpaired T-test. **F,** $Drd2^{Pet1\text{-}CKO}$ nucleus size (area used to quantify puncta levels) does not differ in males (n= 6 males) versus females (n= 4 females), p=0.3497, unpaired T-test. Error bars indicate SEM throughout. For E and F, larger symbols outlined in black represent animal averages used for statistical analysis, smaller symbols represent individual cells, matched in color to the average.

Figure 8. ***Drd2-Pet1* neuron electrophysiological properties in male versus female mice.** Membrane and action potential characteristics were analyzed in GFP-marked *Drd2-Pet1* male and female neurons using whole-cell patch clamp electrophysiology in acute brain slices from triple transgenic *Drd2::cre, Pet1::Flpe, RC::FrePe* mice. (**A**) Membrane potential, (**B**) membrane resistance, (**C**) action potential threshold, (**D**) action

potential amplitude and (**F**) afterhyperpolarization amplitude do not differ in male (n=19) or female (n=44) *Drd2-Pet1* neurons while (**E**) male *Drd2-Pet1* neurons had a significantly longer (2.847 ± 0.155 ms, n=19 cells) action potential duration than in females (2.54 ± 0.094 ms, n=44 cells, p=0.0275, unpaired T-test).

Figure 9. *Drd2-Pet1* neuron axon terminals target brain regions involved in sensory processing and defensive behavior in both male and female mice. A, Intersectional genetic strategy: expression of *Drd2-Cre and Pet1-Flpe* transgenes results in dual recombination of intersectional allele, *RC-FPSit,* to label boutons of *Drd2-Pet1* neurons with Synaptophysin-GFP. **B,** Representative images of *Drd2-Pet1* boutons in the superior olivary complex (SOC) and inferior colliculus (IC). GFP+ (green, marked with arrows) boutons co-localize with 5-HT (magenta) staining. DAPI-stained nuclei shown in blue. Scale bar 25 μm. **C,** Quantification of the percent target area occupied by projections for all ten brain regions examined, see methods for quantification protocol. Target areas analyzed include brain regions involved in auditory processing and social behavior including the cochlear nucleus (CNC), superior olivary complex (SOC), lateral lemniscus (LL), inferior colliculus (IC), caudal pontine reticular nucleus (PNC), medial habenula (mHb), dorsolateral geniculate nucleus (dLGN), medial preoptic area (mPOA), and periaqueductal gray (PAG). The dorsal paragigantocellular nucleus (DPGi) was also examined. No significant differences in projection area innervation were observed between males (n=5) and females (n=6). **D,** Example graph showing correlation between innervation density of auditory brain regions differs in males compared to females. Each dot represents one animal. Values are shown as Pearson's correlation coefficient (r) and * indicates $P < 0.5$ in a two-tailed test. **E,**

1185 Pairwise correlations shown for male and female innervation density in auditory brain
1186 regions. Heatmaps represent high correlation (green) and low correlation (black)
1187 between CNC, SOC, LL, IC and PNC.

1188 **Figure 10. GABA immunoreactivity localizes to soma, but not axonal projections,**
1189 **of *Drd2-Pet1* neurons. A,** GABA staining (magenta) co-localizes with many *Drd2-Pet1*
1190 neuron soma (green GFP-positive cell bodies in *Drd2-Cre;Pet1-Flpe;RC-FPSit* mice) in
1191 the DR in a punctate manner (top), inset of boxed region showing neuron soma positive
1192 for GFP and GABA. Some *Drd2-Pet1* neuron soma are immuno-negative for GABA
1193 (bottom). Dotted lines encircle GFP-positive cell body. **B-C,** No GFP-positive *Drd2-Pet1*
1194 boutons (green) co-localize with GABA staining (magenta) in brain regions examined,
1195 shown here, representative images from SOC (**B**) and IC (**C**), noting a GABA-positive
1196 soma is visible in the image of the IC. **D,** GABA-positive immunoreactivity in the corpus
1197 callosum demonstrating detection of GABA boutons. ChAT (white) staining was used
1198 throughout for anatomical localization. Scale bars 25μm in left panel, 10 μm in inset.
1199 DAPI-stained nuclei shown in blue.

1200 **Table 1. Settings for *Gad2* quantification in *Drd2*$^{Pet1\text{-}CKO}$ tissue.** Summary of settings
1201 and performance in a linear regression for semi-automated protocol versus hand counts
1202 for each FISH probe.

1203 **Table 2. Statistical analysis.** Statistical values are provided for behavioral analyses of
1204 *Drd2*$^{Pet1\text{-}CKO}$ mice and comparison of *Drd2-Pet1* neuron properties in male versus female
1205 mice. Figure numbers are included to reference corresponding graphs. Statistical
1206 analyses were conducted in GraphPad Prism Version 8.1. Statistically significant results
1207 are colored in red.

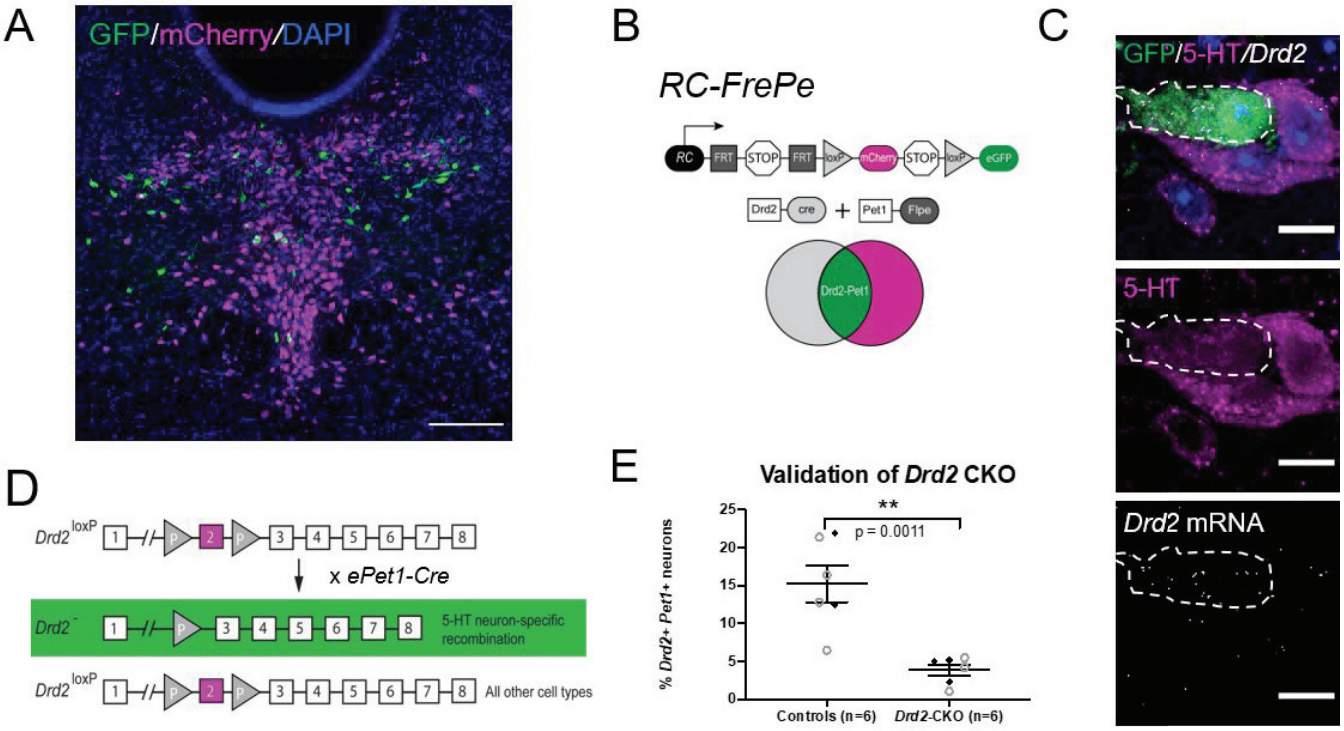

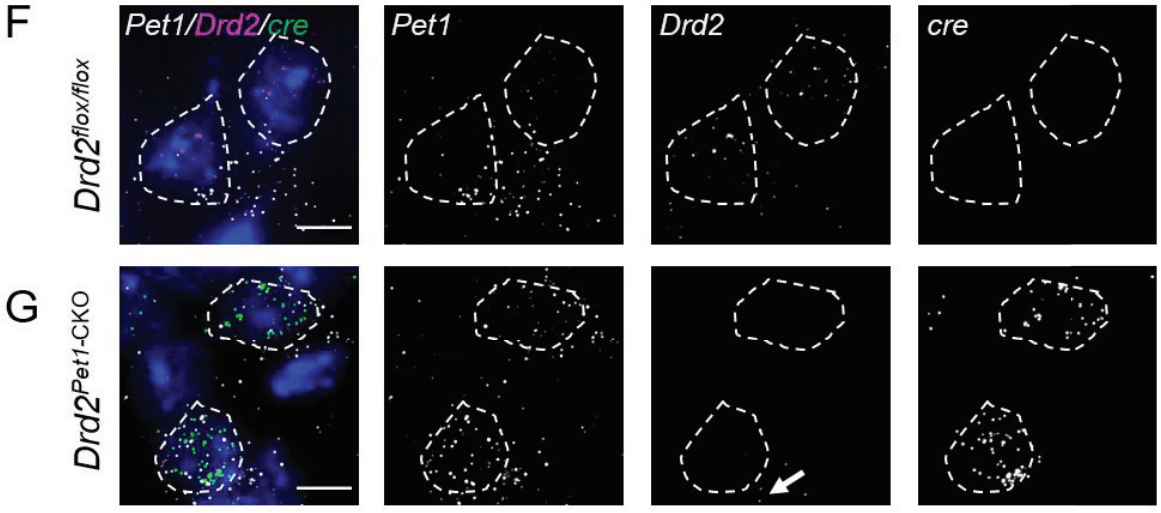

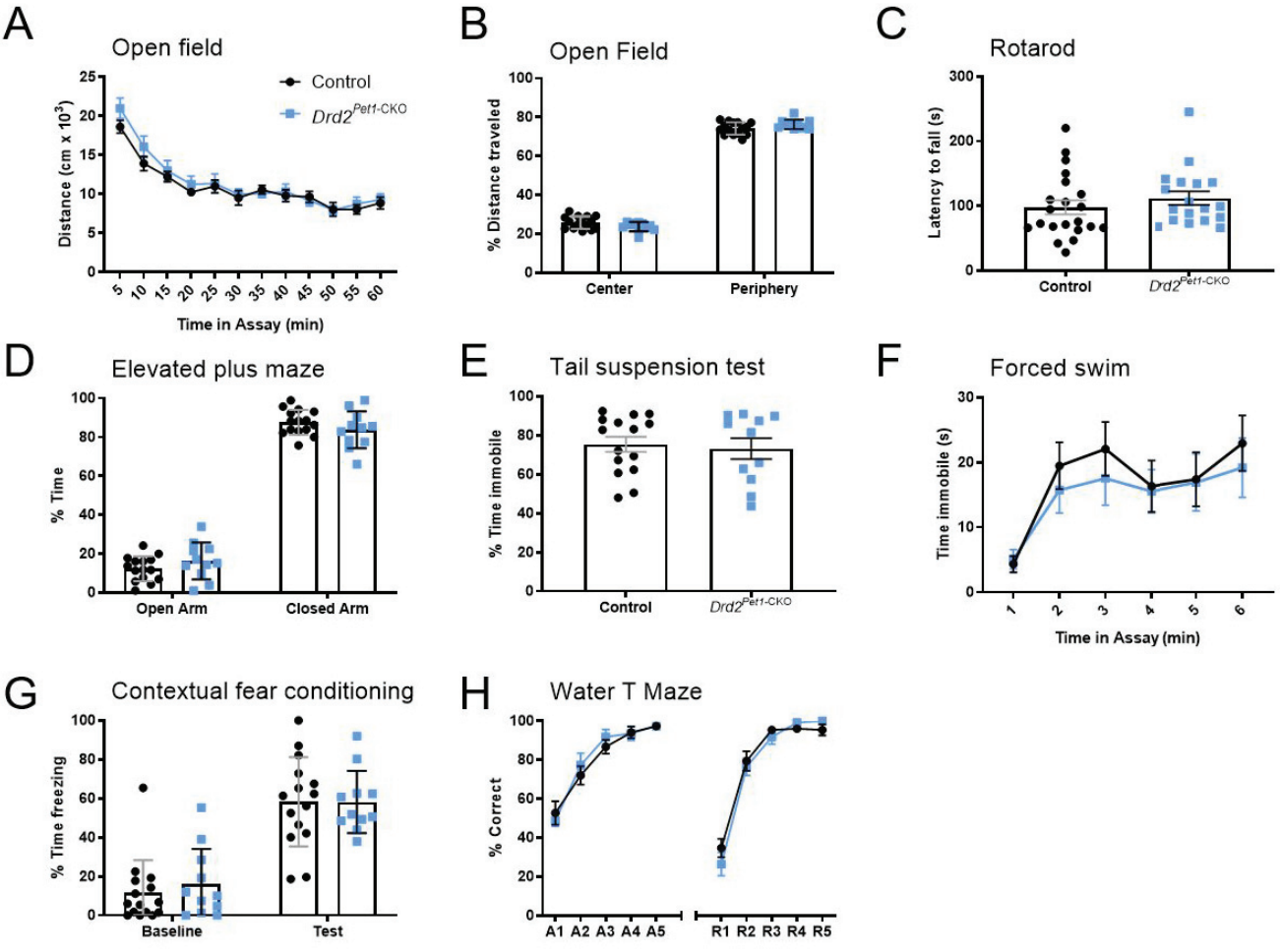

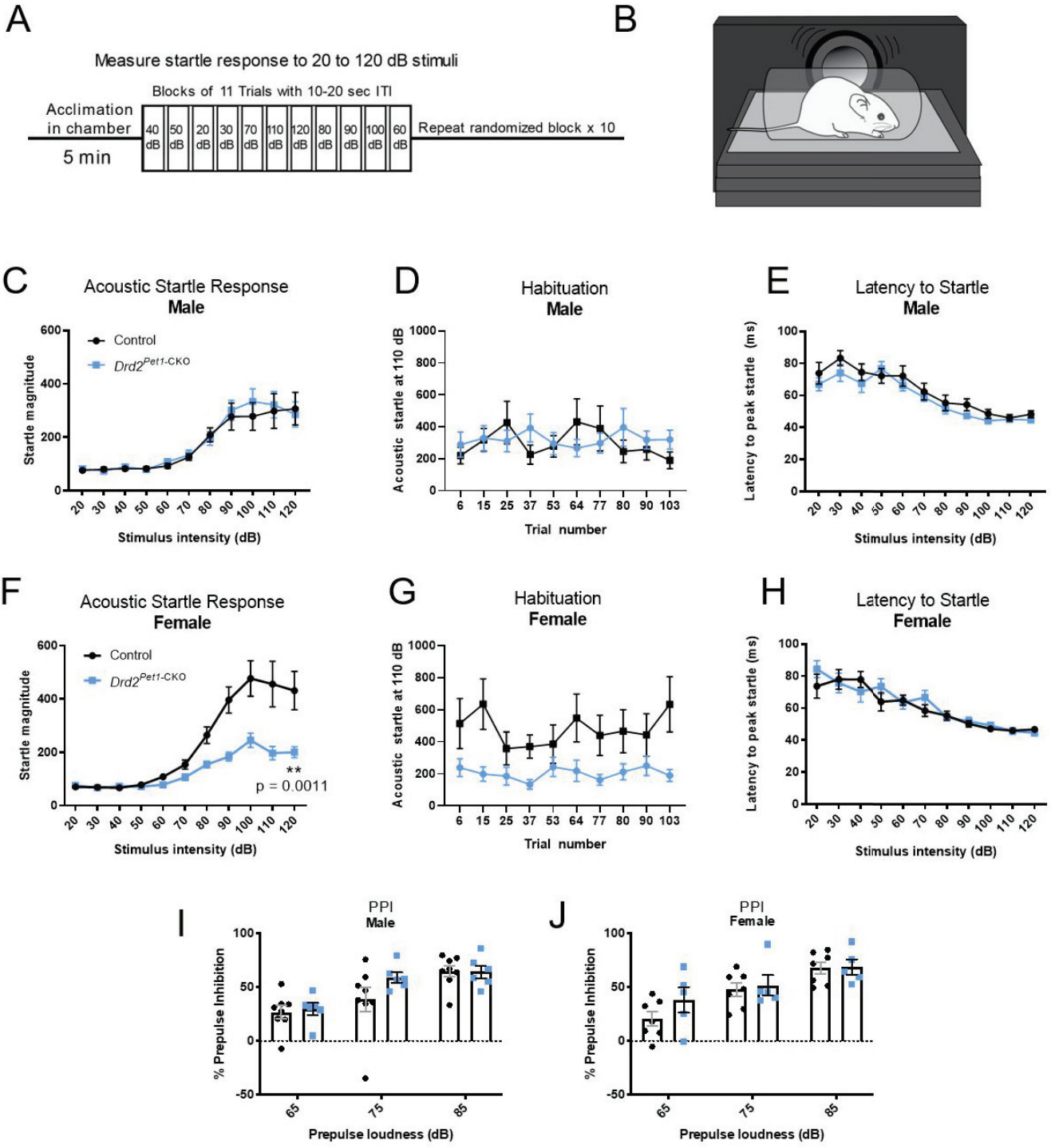

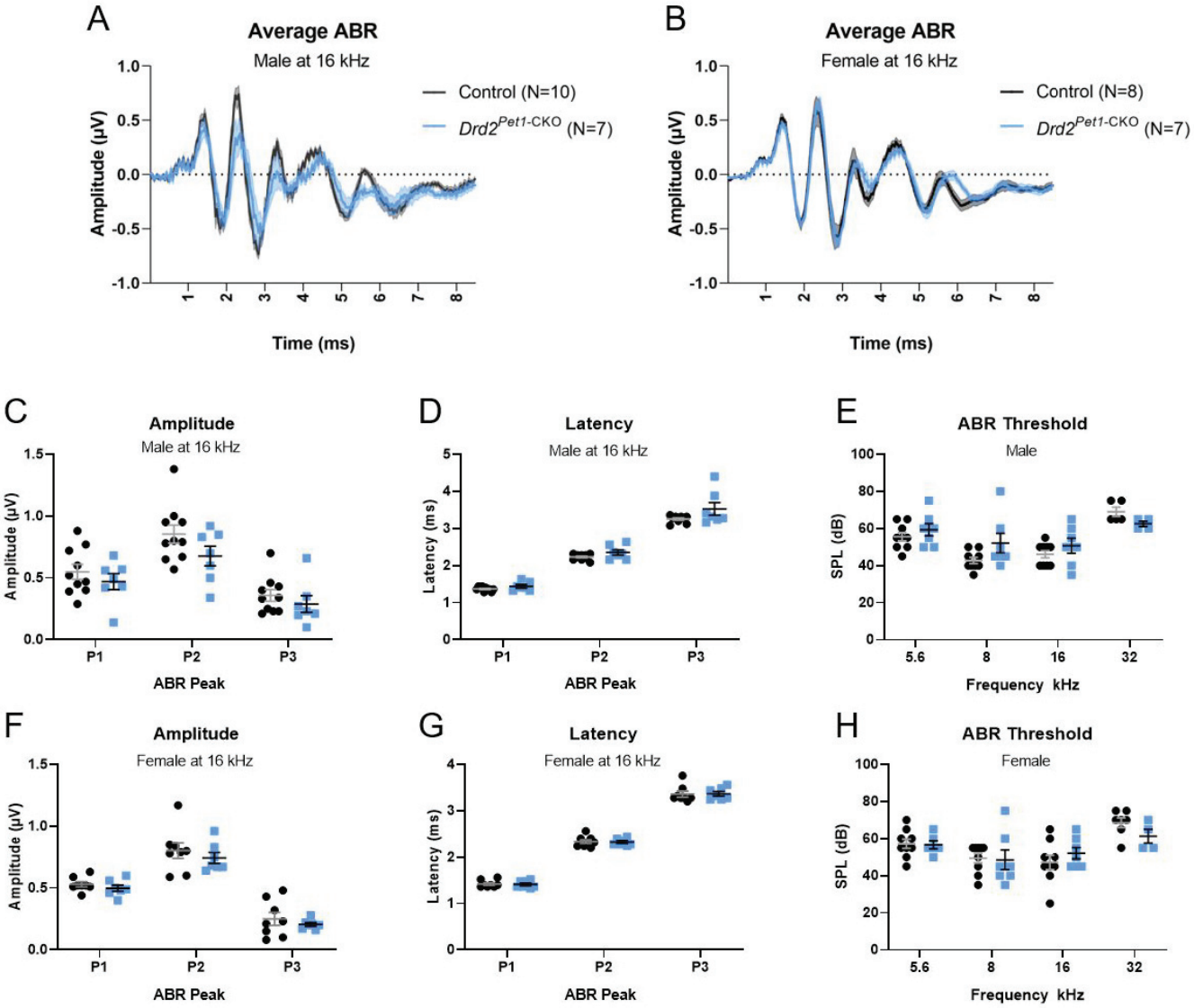

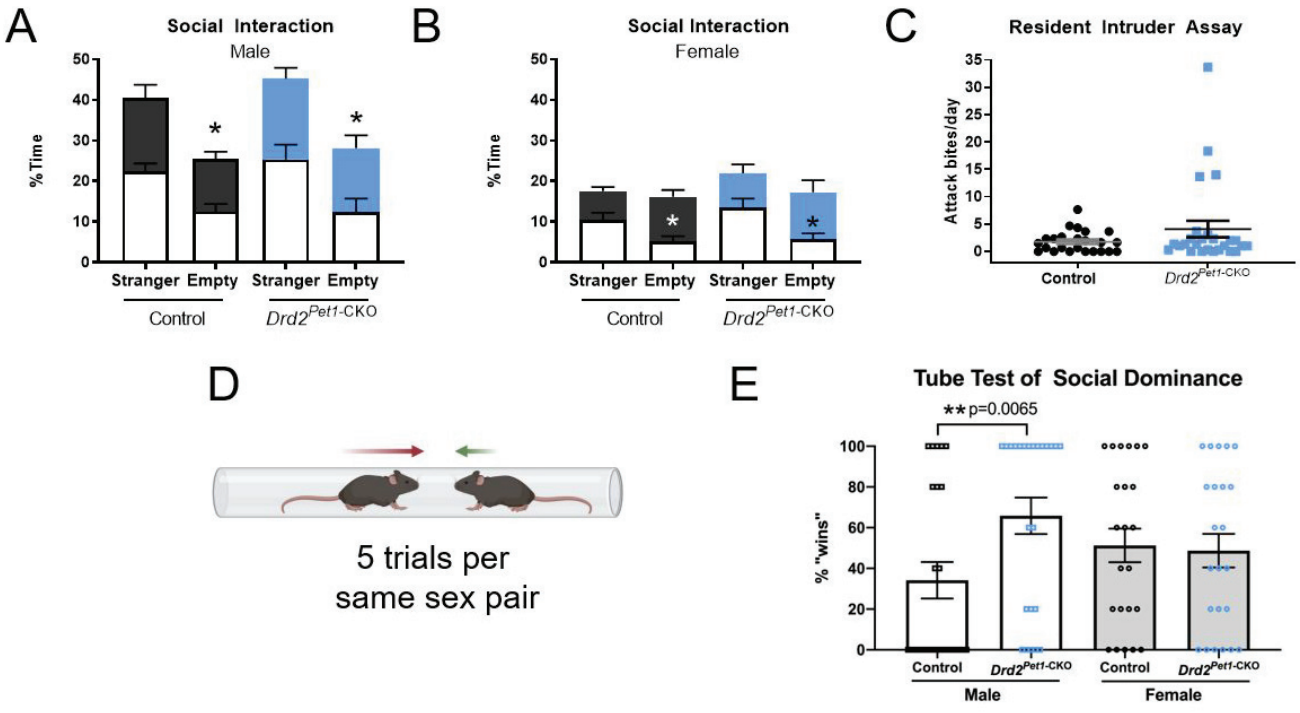

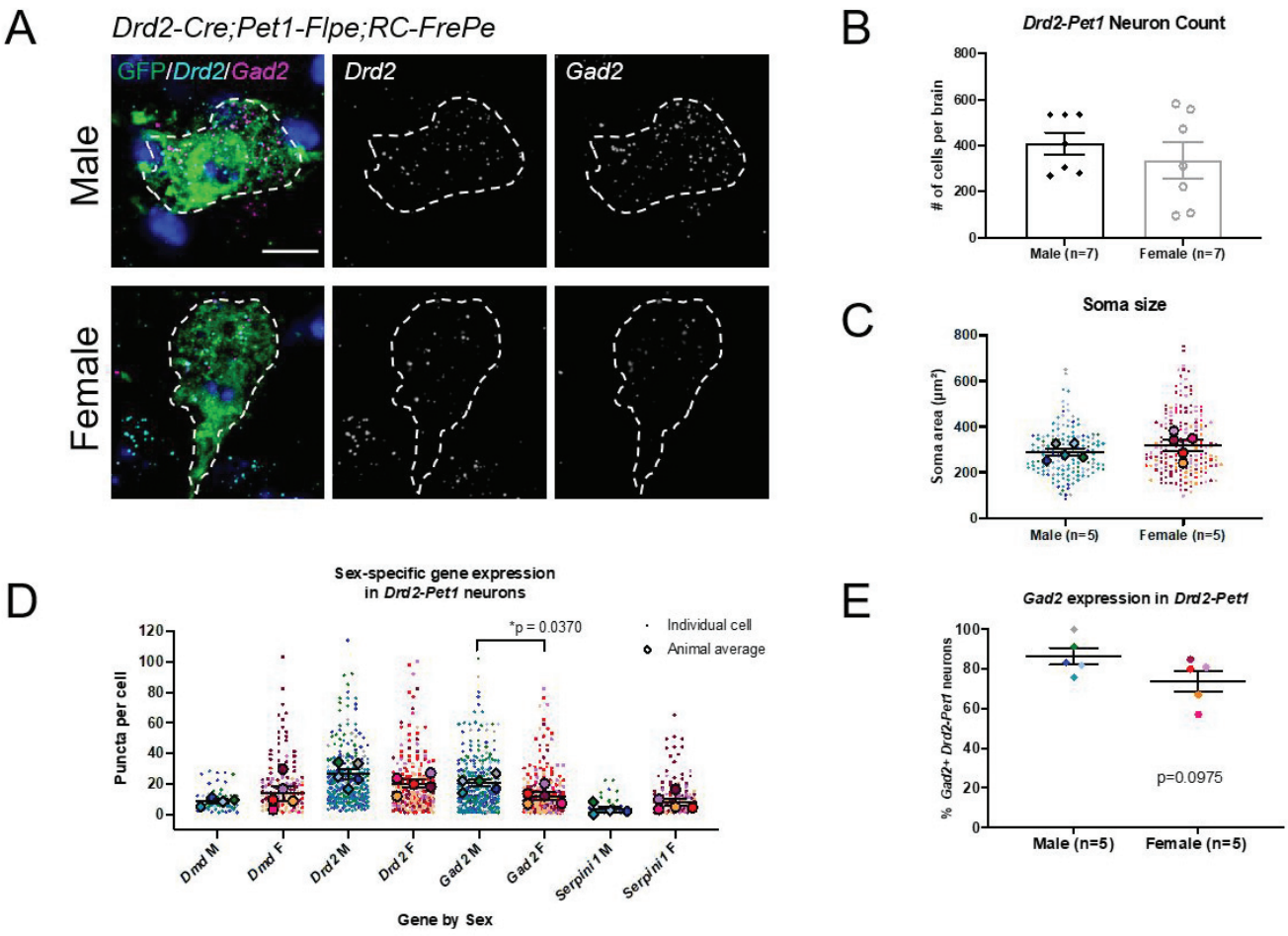

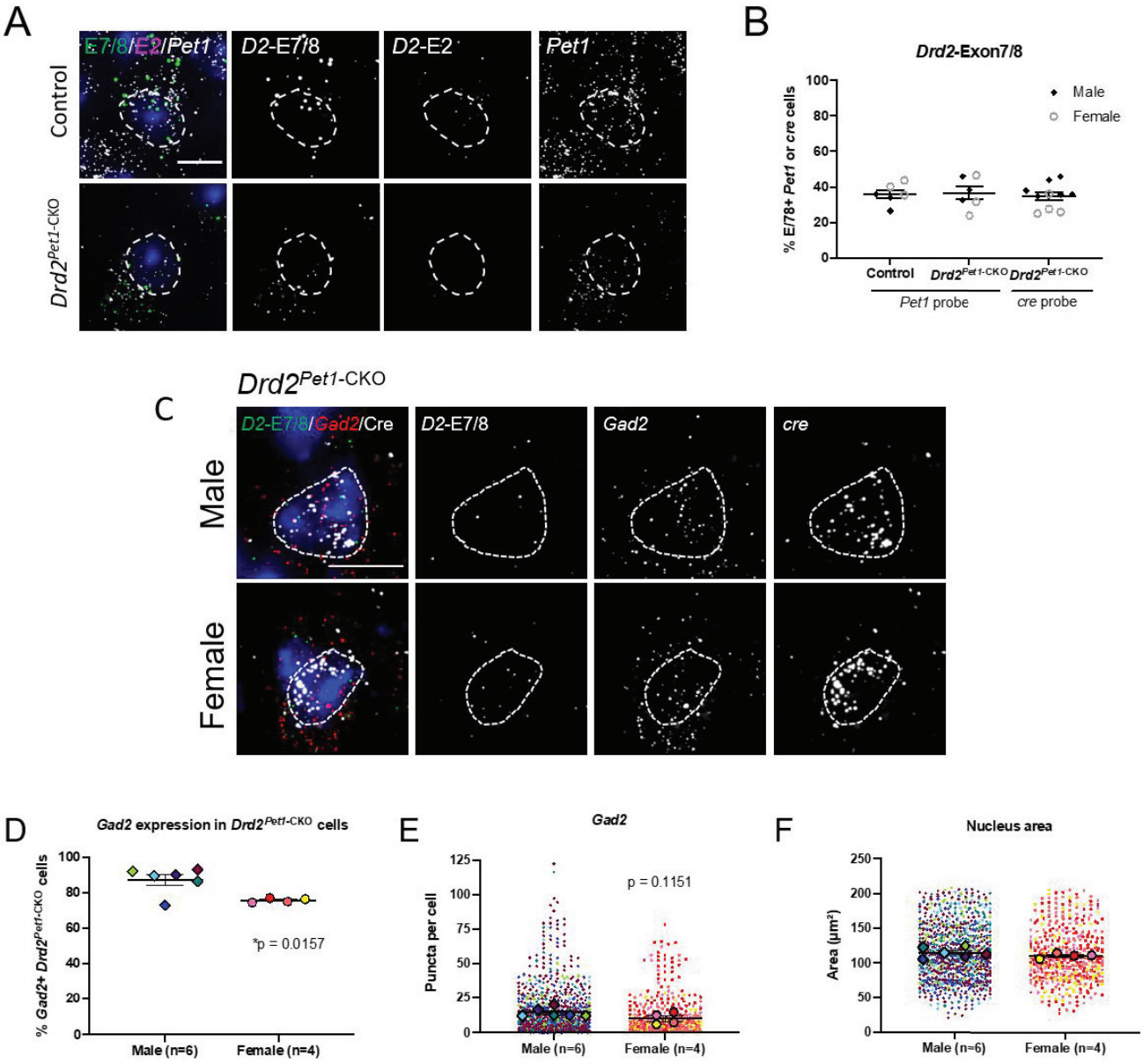

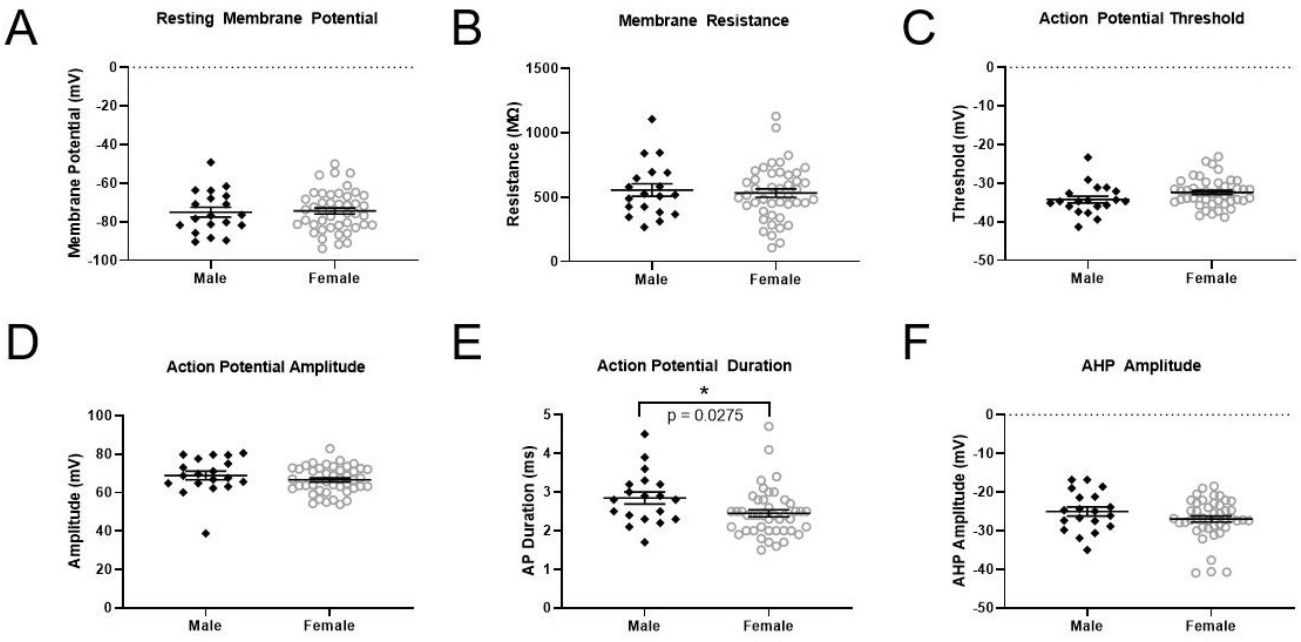

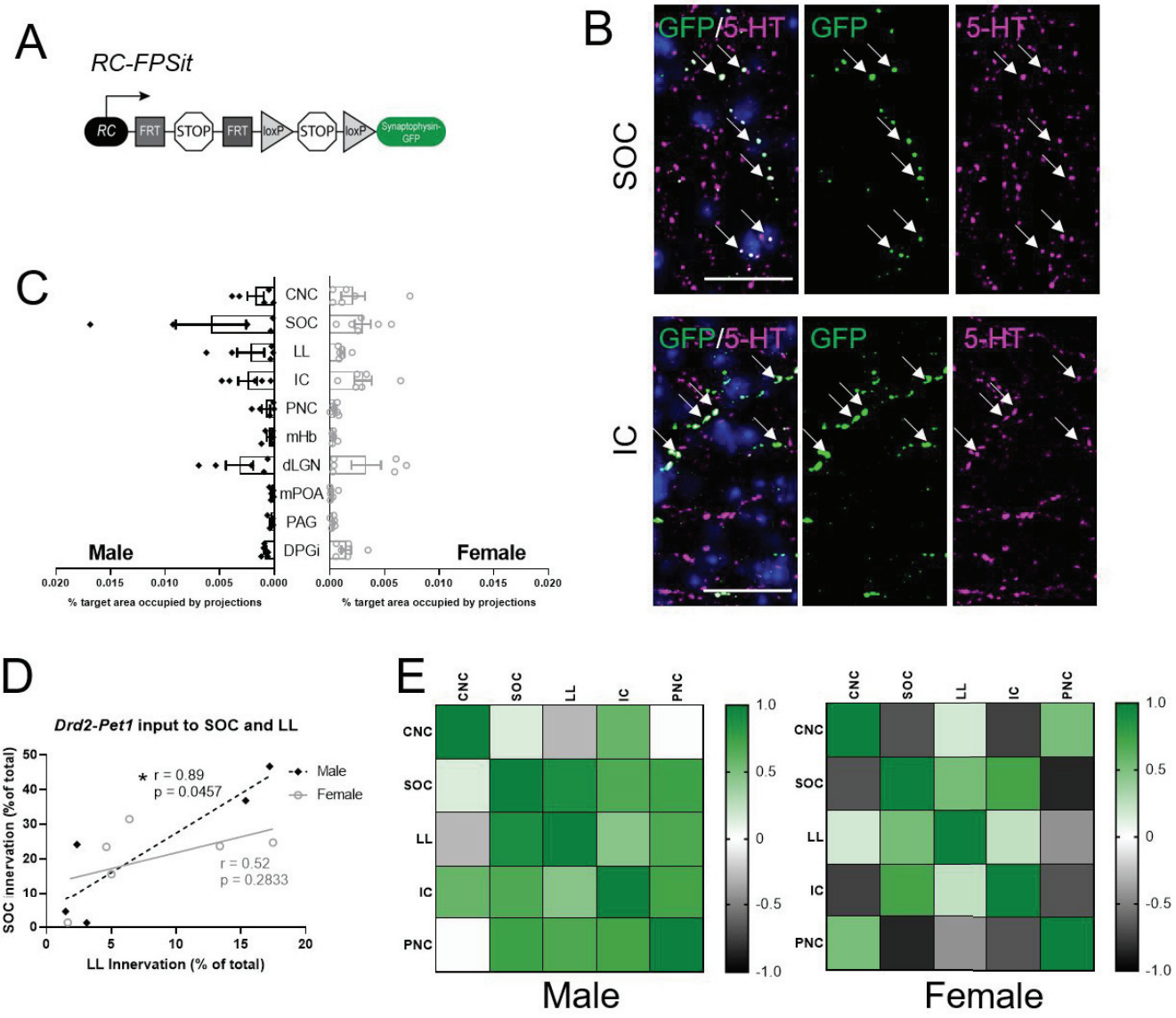

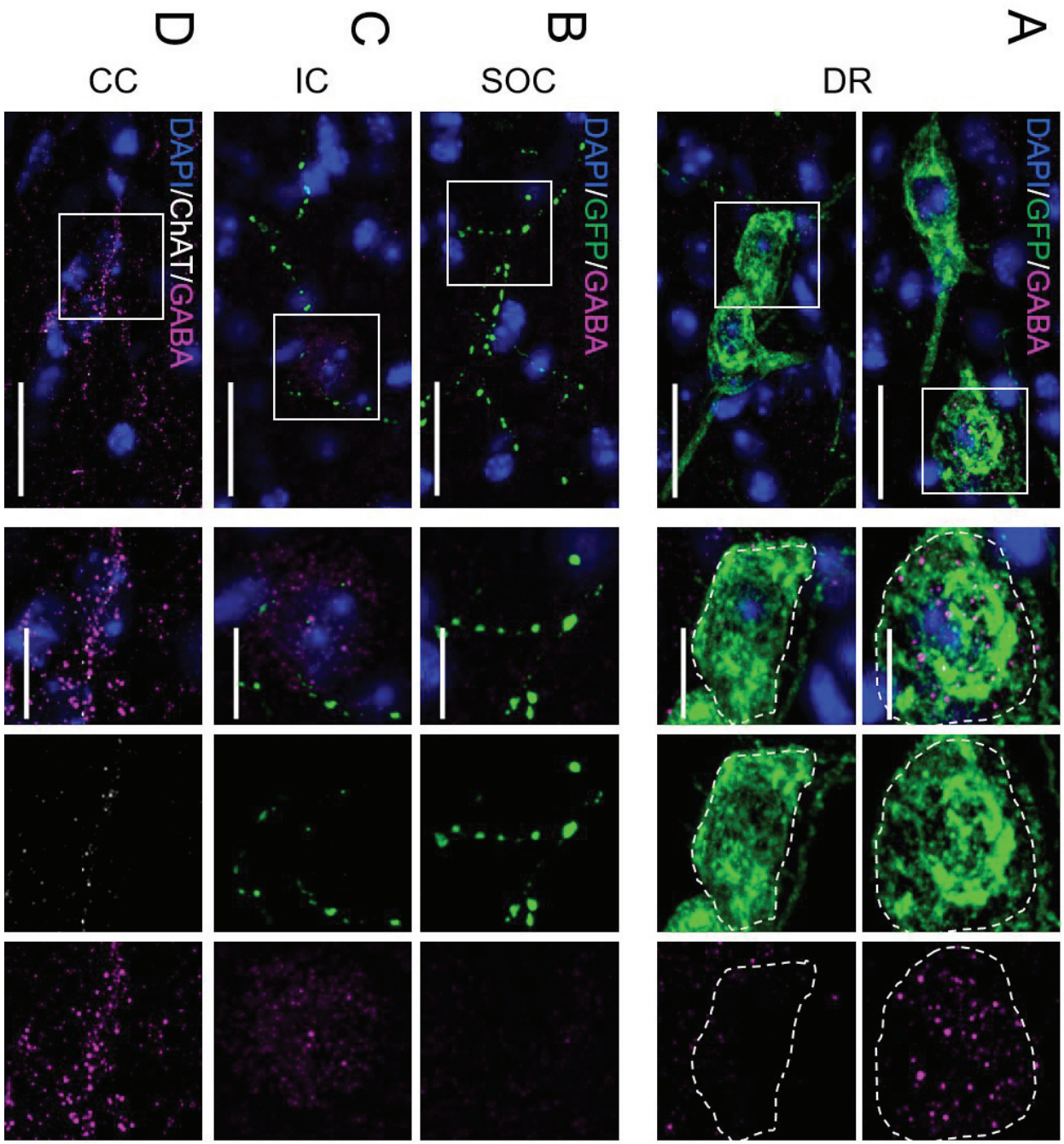

Probe	S1	S2	Prominence	R^2	RMSE	MAE
E2	0.25	1	175	0.8696	0.5957	0.2458
E7/8	0.5	1	100	0.9421	0.8054	0.35
Cre	0.5	1	100	0.9679	3.829	2.2244
Fev	0.25	2	75	0.9555	4.414	3.7047
Gad2	0.25	16	150	0.8568	2.804	1.7973

Behavior/experiment	Line	Data structure (normality)	Type of test	Power		
				Comparison	F/df	p
Validation of *Drd2* CKO	1E	Yes	unpaired T-test	control vs *Drd2*$^{Pet1\text{-}CKO}$	t=4.514, df=10	p=0.0011
Open field distance	2A	Yes	repeated measures ANOVA	F1- genotype	F (1, 24) = 0.6405	p=0.4314
				F2 - time	F (11, 264) = 47.99	p<0.0001
				(F1 x F2)	F (11, 264) = 0.8441	p=0.5960
Open field % distance traveled in center	2B	Yes	unpaired T-test	control vs *Drd2*$^{Pet1\text{-}CKO}$	t=1.781, df=24	p=0.0876
Rotarod	2C	No	Mann-Whitney, two-tailed	control vs *Drd2*$^{Pet1\text{-}CKO}$	M-W U=142	p=0.1899
Elevated plus maze (% time in open arm)	2D	Yes	unpaired T-test	control vs *Drd2*$^{Pet1\text{-}CKO}$	t=1.250, df=24	p=0.2234
Tail suspension test	2E	Yes	unpaired T-test	control vs *Drd2*$^{Pet1\text{-}CKO}$	t=0.3485, df=24	p=0.7305
Forced swim test	2F	Yes	repeated measures ANOVA	F1- genotype	F (1, 24) = 0.2678	p=0.6095
				F2 - time	F (5, 120) = 8.916	p<0.0001
				(F1 x F2)	F (5, 120) = 0.3090	p=0.9067
Contextual fear conditioning (Baseline freezing)	2G	Yes	unpaired T-test	control vs *Drd2*$^{Pet1\text{-}CKO}$	t=0.6682, df=24	p=0.5104
Contextual fear conditioning (Test freezing)			unpaired T-test	control vs *Drd2*$^{Pet1\text{-}CKO}$	t=0.0127, df=24	p=0.9900
Water T maze (%correct during acquisition)	2H	Yes	repeated measures ANOVA	F1- genotype	F (1, 24) = 0.08249	p=0.7764
				F2 - time	F (4, 89) = 50.12	p<0.0001
				(F1 x F2)	F (4, 89) = 0.6698	p=0.6147
Water T maze (%correct during reversal)		Yes	repeated measures ANOVA	F1- genotype	F (1, 24) = 0.1631	p=0.6899
				F2 - time	F (4, 96) = 172.4	p<0.0001
				(F1 x F2)	F (4, 96) = 1.477	p=0.2153
ASR (M)	3C	Yes	repeated measures ANOVA	F1- genotype	F (1, 25) = 0.0840	p=0.7745
				F2 - dB	F (10, 250) = 28.99	p<0.0001
				(F1 x F2)	F (10, 250) = 0.3037	p=0.9798
ASR Habituation (M)	3D	Yes	Pearson r correlation	control trial number x startle response	r=-0.195	p=0.5893
				Drd2$^{Pet1\text{-}CKO}$ trial number x startle response	r=0.136	p=0.7079
ASR Latency (M)	3E	Yes	repeated measures ANOVA	F1- genotype	F (1, 25) = 2.425	p=0.1319
				F2 - dB	F (10, 250) = 21.67	p<0.0001
				(F1 x F2)	F (10, 250) = 0.4722	p=0.9071
ASR (F)	3F	Yes	repeated measures ANOVA	F1- genotype	F (1, 29) = 13.26	p=0.0011
				F2 - dB	F (10, 29) = 35.29	p<0.0001
				(F1 x F2)	F (10, 290) = 7.475	p<0.0001
ASR Habituation (F)	3G	Yes	Pearson r correlation	control trial number x startle response	r=0.1171	p=0.7473
				Drd2$^{Pet1\text{-}CKO}$ trial number x startle response	r=0.05165	p=0.8873
ASR Latency (F)	3H	Yes	repeated measures ANOVA	F1- genotype	F (1, 29) = 0.3748	p=0.5452
				F2 - dB	F (10, 290) = 20.59	p<0.0001
				(F1 x F2)	F (10, 290) = 1.058	p=0.3953
PPI (M)	3I	Yes	repeated measures	F1- genotype	F (1, 12) = 0.6625	p=0.4315
				F2 -prepulse dB	F (2, 24) = 42.86	p<0.0001

			ANOVA	(F1 x F2)	F (2, 24) = 4.104	p=0.0293
PPI (F)	3J	Yes	repeated measures ANOVA	F1- genotype	F (1, 10) = 0.6526	p=0.4380
				F2 -prepulse dB	F (2, 20) = 31.34	p<0.0001
				(F1 x F2)	F (2, 20) = 1.609	p=0.2249
ABR Amplitude (M)	4C	Yes	repeated measures ANOVA	F1- genotype	F (1, 15) = 1.770	p=0.2032
				F2- peak	F (2, 30) = 59.09	p<0.0001
				(F1 x F2)	F (2, 30) = 1.059	p=0.3595
ABR Latency (M)	4D	Yes	repeated measures ANOVA	F1- genotype	F (1, 15) = 3.515	p=0.0804
				F2- peak	F (2, 30) = 1171	p<0.0001
				(F1 x F2)	F (2, 30) = 3.121	p=0.0587
ABR Threshold (M)	4E					
5.6		Yes	unpaired T-test	control vs *Drd2*$^{Pet1\text{-}CKO}$	t=0.9535, df=14	p=0.3565
8		Yes	unpaired T-test	control vs *Drd2*$^{Pet1\text{-}CKO}$	t=1.894, df=14	p=0.0791
16		Yes	unpaired T-test	control vs *Drd2*$^{Pet1\text{-}CKO}$	t=1.103, df=14	p=0.2887
32		Yes	unpaired T-test	control vs *Drd2*$^{Pet1\text{-}CKO}$	t=2.129, df=7	p=0.0708
ABR Amplitude (F)	4F	Yes	repeated measures ANOVA	F1- genotype	F (1, 13) = 2.489	p=0.1387
				F2- peak	F (2, 26) = 72.52	p<0.0001
				(F1 x F2)	F (2, 26) = 0.0487	p=0.9525
ABR Latency (F)	4G	Yes	repeated measures ANOVA	F1- genotype	F (1, 13) = 0.0053	p=0.9430
				F2- peak	F (2, 26) = 4360	p<0.0001
				(F1 x F2)	F (2, 26) = 0.0822	p=0.9213
ABR Threshold (F)	4H					
5.6		Yes	unpaired T-test	control vs *Drd2*$^{Pet1\text{-}CKO}$	t=0.1566, df=13	p=0.8770
8		Yes	unpaired T-test	control vs *Drd2*$^{Pet1\text{-}CKO}$	t=0.1592, df=14	p=0.8757
16		Yes	unpaired T-test	control vs *Drd2*$^{Pet1\text{-}CKO}$	t=0.9600, df=14	p=0.3533
32		Yes	unpaired T-test	control vs *Drd2*$^{Pet1\text{-}CKO}$	t=1.644, df=9	p=0.1346
Social Interaction (M, %time with stranger)	5A	Yes	unpaired T-test	control vs *Drd2*$^{Pet1\text{-}CKO}$	t=0.6283, df=12	p=0.5415
Social Interaction (F, %time with stranger)	5B	Yes	unpaired T-test	control vs *Drd2*$^{Pet1\text{-}CKO}$	t=0.9598, df=10	p=0.3598
Resident Intruder Assay	5C	No	Mann-Whitney, two-tailed	control vs *Drd2*$^{Pet1\text{-}CKO}$	M-W U=289.5	p=0.6649
Tube Test of Social Dominance	5E					
male		No	Mann-Whitney, two-tailed	control vs *Drd2*$^{Pet1\text{-}CKO}$	M-W U=166	p=0.0065
female		No	Mann-Whitney, two-tailed	control vs *Drd2*$^{Pet1\text{-}CKO}$	M-W U=253	p=0.8123
Drd2-Pet1 Neuron Count	6A	Yes	unpaired T-test	male vs female	t=0.8160, df=12	p=0.4304
Soma size	6C	Yes	unpaired T-test	male vs female	t=1.021, df=8	p=0.3372
Gene expression	6D					
Dmd		Yes	unpaired T-test	male vs female	t=0.9581, df=7	p=0.3699
Drd2		Yes	unpaired T-test	male vs female	t=1.514, df=8	p=0.1686
Gad2		Yes	unpaired T-test	male vs female	t=2.498, df=8	p=0.0370
Serpini1		Yes	unpaired T-test	male vs female	t=1.459, df=7	p=0.1879
%Gad2+ Drd2-Pet1 neurons	6E	Yes	unpaired T-test	male vs female	t=1.876, df=8	p=0.0975
% *Drd2*-Exon7/8+	7B	Yes	unpaired T-test	control vs *Drd2*$^{Pet1\text{-}CKO}$ with *Pet1*	t=0.1291, df=10	p=0.8998

				probe		
		Yes	one-way ANOVA	control/*Pet1* probe vs *Drd2*$^{Pet1\text{-}CKO}$/*Pet1* probe vs *Drd2*$^{Pet1\text{-}CKO}$/Cre probe	F (2, 19) = 0.1003	p=0.9051
% *Gad2* in Cre+ neurons	7D	Yes	unpaired T-test	male vs female	t=3.057, df=8	p=0.0157
Gad2 punctae per cell	7E	Yes	unpaired T-test	male vs female	t=1.768, df=8	p=0.1151
Nucleus area	7F	Yes	unpaired T-test	male vs female	t=0.9931, df=8	p=0.3497
Resting membrane potential	8A	Yes	unpaired T-test	male vs female	t=0.2113, df=61	p=0.8334
Membrane resistance	8B	Yes	unpaired T-test	male vs female	t=-0.4084, df=61	p=0.6844
Action potential threshold	8B	Yes	unpaired T-test	male vs female	t=1.8197, df=61	p=0.0737
Action potential amplitude	8D	Yes	unpaired T-test	male vs female	t=-1.0474, df=61	p=0.2990
Action potential duration	8E	Yes	unpaired T-test	male vs female	t=-2.2583, df=61	p=0.0275
AHP amplitude	8F	Yes	unpaired T-test	male vs female	t=1.350, df=61	p=0.1821
Innervation densities	9C					
DPGi		Yes	unpaired T-test	male vs female	t=1.285, df=9	p=0.2308
PAG		Yes	unpaired T-test	male vs female	t=0.2398, df=9	p=0.8158
mPOA		Yes	unpaired T-test	male vs female	t=0.1978, df=9	p=0.8476
DLG		Yes	unpaired T-test	male vs female	t=0.07798, df=9	p=0.9395
mHb		Yes	unpaired T-test	male vs female	t=0.6732, df=9	p=0.5178
PnC		Yes	unpaired T-test	male vs female	t=0.7901, df=9	p=0.4498
IC		Yes	unpaired T-test	male vs female	t=0.5350, df=9	p=0.6056
LL		Yes	unpaired T-test	male vs female	t=0.9100, df=9	p=0.3865
SOC		Yes	unpaired T-test	male vs female	t=0.9282, df=9	p=0.3775
CNC		Yes	unpaired T-test	male vs female	t=0.2997, df=9	p=0.7712